A simple circularity-based approach for nanoparticle size histograms beyond the spherical approximation

Florent Tournus

Ultramicroscopy 268 (2025) 114067

Contents lists available at ScienceDirect

Ultramicroscopy

journal homepage: www.elsevier.com/locate/ultramic

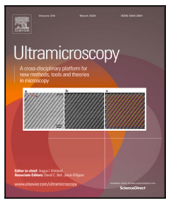

A simple circularity-based approach for nanoparticle size histograms beyond the spherical approximation

Florent Tournus

Université de Lyon, Université Claude Bernard Lyon 1, CNRS, Institut Lumière Matière, F-69622, Villeurbanne, France

ARTICLE INFO

Keywords:
Nanoparticles
Size histogram
Electron microscopy
Cluster deposition
Nanoparticle shape
Particle assembly

ABSTRACT

Conventional Transmission Electron Microscopy (TEM) is widely used for routine characterization of the size and shape of an assembly of (nano)particles. While the most basic approach only uses the projected area of each particle to infer its size (the "circular equivalent diameter" corresponding to the so-called "spherical approximation"), other shape descriptors can be determined and used for more elaborate analyses. In this article we present a generic model of particles, considered to be made of a few individual grains, and show how the equivalent size (i.e. a particle volume information) can be reliably deduced using only two basic parameters: the projected area and the perimeter of a particle. We compare this simple model to the spherical and ellipsoidal approximations and discuss its benefits. Then, partial coalescence of grains in a particle is also considered and we show how a simple analytical approximation, based on the circularity parameter of each particle, can improve the experimental determination of a particle size histogram. The analysis of experimental observations on nanoparticles assemblies obtained by mass-selected cluster deposition is presented, to illustrate the efficiency of the proposed approach for the determination of particle size just from conventional TEM images. We show how the presence of multimers offers an excellent opportunity to validate our improved and simple procedure. In addition, since the circularity plays a central role in this approach, attention is attracted on the perimeter determination in a pixelated image.

1. Introduction

Nanoparticles are of great interest in a wide range of disciplines [1–11], going from chemistry and catalysis to biomedicine or geoscience, through various area of physics: optics, magnetism, electronics etc. There exists many ways to artificially produce nanoparticle samples, while nature is also able to provide nanoparticles of different kinds (for instance due to combustion/volcanism [6,12] or to living beings...). From a characterization point of view it is often essential to be able to determine the shape and size distribution in an assembly of nanoparticles (or microparticles as well, the approach exposed in this paper can in fact be applied at any scale) [6,13–17], for instance in the precise case of size-effect investigations for nano-magnets [18–27]. A method of choice, quite easily accessible, is to observe an assembly of dispersed particles on a surface with conventional Transmission Electron Microscopy (TEM) [6,28–32]. This is a powerful technique, with an excellent spatial resolution, no problem of probe convolution (contrary to scanning electron microscopy (SEM) which is also often used, especially for large particles) [15,30,33,34], and with a direct visualization of the particles in the sample (as opposed to indirect methods using scattering of X-rays or visible light for instance...) thus providing a lot of information: the particle arrangement in the sample, the variability of size and shape etc. Image analysis procedures and particle classification have thus been devised, sharing common questions with other techniques of imaging (optical microscopy or SEM for instance) and in connection with many fields of research at the micro or macro-scale (volcanology, geology, sedimentary research, crop science, metrology and computer vision in general) [35–48].

However, except when more involved techniques are used (tomography in particular), conventional TEM images on assemblies of particles only provide a 2D information, namely we can separate in a image the particles from the background, in order to determine their projected area, but *out-of-plane information* (i.e. along the observation direction) is missing. Note that the contrast of a particle, while it has a dependence on its thickness, cannot be reliably and routinely used to determine the volume in an assembly of particles. For such a purpose, one would prefer to use a technique like STEM-HAADF giving somehow access to an out-of-plane information, but also with some limitations (resolution, damage of the particles, chemical sensitivity...), or other techniques more time-consuming and/or harder to apply to a large number of particles (electron/atom probe tomography, holography...) [49–64].

E-mail address: florent.tournus@univ-lyon1.fr.

https://doi.org/10.1016/j.ultramic.2024.114067
Received 23 July 2024; Received in revised form 11 October 2024; Accepted 18 October 2024
Available online 28 October 2024

Therefore, particles characterization using conventional TEM sticks with 2D information and one has to resort to some hypothesis to infer 3D information. Notably, a whole community has been working in this direction with the study of soot particles, consisting in agglomerates of complex shapes (with fractal dimension) made of a large number of primary nanoparticles, aiming at a 3D structure determination from projected area TEM imaging, with the help of computer softwares, simulations and possibly artificial intelligence [6,12,45,65–69]. Since the notion of *particle size* is in fact usually related to the particle volume, especially for comparison with different measurements and experimental techniques (for instance magnetometry measurements in the precise case of nanomagnets [18,19,22,23], as the particles considered in Section 4), it is highly desirable to have access to a reliable evaluation of the volume. The simplest and common approximation is to consider that particles are spherical, and then infer their equivalent size from the projected area A only: this hypothesis means that the out-of-plane dimension of an observed particle is equal to the diameter D_{sph} of the disk having the area A. This may be a reasonable assumption in the case of particles which *look* spherical, i.e. which are *circular* (however it is always possible that the particles are for instance flat disks...). But what about particles having irregular shapes, for which the spherical hypothesis would be obviously wrong?

In the present article, our motivation is to provide a simple approach for the analysis of the particle size distribution going beyond the crude spherical approximation. In Section 2, in addition to the spherical and ellipsoidal hypotheses, we present a generic model of particles, considered to be made of individual grains. We show how the *equivalent diameter* is related to two basic parameters: the projected area A and the perimeter P of each particle. Then, in Section 3, we introduce a partial coalescence model (quantified by an overlap parameter) extending the "grain" model, which allows us to improve the particle size determination especially when A vs. P displays a linear trend. We establish a simple analytical approximation for the inferred *out-of-plane dimension*, where the *circularity* appears as a central parameter to correct the diameter from the spherical hypothesis. In Section 4 the approach is illustrated on various samples of deposited clusters, where convention TEM images are used to compute the particle size distribution. The efficiency of the partial coalescence approximation is discussed and in particular we take benefit from the presence of multimers on the surface (i.e. particles made of two or more incident clusters that have come into contact [20,70]) to validate our improved procedure. In addition, since the circularity plays a central role in this approach, attention is attracted on the perimeter determination in a pixelated image. Finally, a summary and conclusion is given in the last section.

2. Basic models and their relation with shape parameters

2.1. Concept of equivalent diameter and spherical approximation

In a very general way, one can defined the equivalent diameter of any particle (of any shape) as the diameter of a sphere having the same volume as the true particle volume V:

$$D_{eq} = \left(\frac{6V}{\pi}\right)^{1/3} \tag{1}$$

If the volume V can be measured, then the equivalent diameter is non-ambiguously defined (it is sometimes called "volume equivalent diameter" [71]). Since all the difficulty is that precisely we do not have access to the particle volume, in the following discussion the equivalent diameter will be computed using different approximations for the calculation of V from the particle shape analysis (in particular, based on the area and perimeter measurement).

The simplest and widespread hypothesis is what we call the "spherical approximation", where the particle size is determined using only its projected area A. The projected area A of a sphere of diameter D is $A = \frac{\pi}{4}D^2$ and its volume is $V = \frac{\pi}{6}D^3$, then we can call D_{sph} the "equivalent diameter" in the spherical approximation the quantity (sometimes called "Heywood diameter", "circular equivalent diameter" or ECD for "equivalent circular diameter" [14,15,30,33,38,44,46,47,56,58,60,72–76] :

$$D_{sph} = \sqrt{4A/\pi} \tag{2}$$

Note that sometimes a particle diameter is reported without explicitly indicating that this spherical hypothesis has been used and while the particles are apparently not ideal spheres [24–27,29,77,78]. The corresponding volume, directly determined from the area A, is

$$V_{sph} = \frac{2}{3}AD_{sph} = \frac{4}{3\sqrt{\pi}}A^{3/2} \tag{3}$$

Therefore, in this spherical approximation, the equivalent diameter is the one of a perfect sphere having the same projected area A as the one measured for the real particle. Using this particle size to infer the particle volume is equivalent to consider that D_{sph} is also the out-of-plane diameter (maximum particle thickness). Because the spherical shape is an extreme case (point contact with the surface, with absolutely no wetting) one can expect that the V_{sph} value is overestimating the true particle volume V. Moreover, in the case of complex/irregular in-plane shapes obviously deviating from a disk, it can be clear that assuming an out-of-plane dimension of D_{sph} is a wrong estimation of the typical particle thickness. This means that D_{sph} is somehow an upper bound of the correct equivalent diameter.

Let us however emphasize that the "spherical approximation" is a quite natural way to determine a particle size (i.e. a diameter) if the only information available is the projected area A (D_{eq} can also be sometimes called the *area-equivalent diameter* [79]). In addition to its simplicity, this hypothesis is motivated by the fact that a sphere is the equilibrium shape for a freestanding fluid particle (because it corresponds to a minimization of the surface energy, for a given total volume). However there are evident reasons for a deviation from this simple model [5,8,80–83] : i) the particles may be in a non-equilibrium state (for instance touching particles that have not coalesced) (ii) for crystalline particles, the surface energy depends on the orientation (atomic planes) so that facetting is expected, leading to polyhedral equilibrium shapes (iii) particles are supported on a substrate (and potentially capped or embedded in another medium) so that interface energies play a role with wetting/truncation effects, affecting the out-of-plane dimension, even if the system is isotropic in plane. While points (i) and (ii) may be directly detected on the 2D images with non-circular shapes of particles (i.e. their areas do not correspond to disks), the truncation (or flattening) problem of point (iii) will not be visible simply looking at the projected areas.

It should be noted that, for some particular purposes, various shape descriptors (as the circularity and roundness, see below) and alternative diameters (or "lengths") can be used to characterize a particle [36,38,39,72,74,75,84]: for instance the concept of Feret diameter (distance between two parallel lines tangent to the projected contour, also known as the caliper diameter ; the minimum Feret diameter being defined as the minimum length of parallel tangents (particle breadth) according to ISO 9276-6) which is of particular relevance for sieving, and other dimensions that may also be of interest (diameter of the largest inscribed or smallest circumscribing circles, Martin's diameter...) will not be considered in this article.

2.2. Ellipsoidal approximation

One can easily improve the shape description of the particles, taking into account deviations of the projected area from a perfect disk. The "ellipsoidal approximation" thus keeps tracks of the anisotropic shape of the projected area by defining an equivalent ellipse [23,35,36,40–42,45,47,72,75,85] having a major axis D_{major} and a minor axis D_{minor} corresponding in our case to the same inertia matrix (2×2 matrix) as the original particle. Note that while there are other ways to define an

approaching ellipse for a given particle, here we force the area of the ellipse to be the same as the one of the particle, so that we can write:

$$A = \frac{\pi}{4} D_{major} D_{minor} \tag{4}$$

To go further, one then considers that the particles can be approximated by an ellipsoid where the unknown out-of-plane dimension is, for simplicity, equal to D_{minor}. Note that this arbitrary assumption [23,46,75] can in fact be justified by two features: first, when the elongated shapes correspond to particles formed by smaller grains in contact with their neighbors (without or with limited subsequent coalescence) then the "thickness" rather corresponds to the smallest in-plane dimension; second, when there is an adhesion energy (interface energy between the particle surface and the substrate) leading to a particle flattening, then it is not favorable to have an ellipsoid with its longest axis perpendicular to the substrate. Of course, it is still possible to experimentally meet some particles where this assumption is in fact not valid (for instance for columnar particles), so that one must always keep a critical view on the inferred particle size distribution. Nevertheless, let us insist on the fact that the ellipsoidal approximation does only require very light data processing (which are currently done in standard analysis softwares) and it encompasses the spherical approximation (if the projected area is a disk, we simply find $D_{major} = D_{minor}$): it is thus a better approximation than the usual spherical approximation and should therefore be preferred.

The volume of the approximated ellipsoid corresponds to

$$V_{ellips} = \frac{\pi}{6} D_{major} D_{minor}^2 = \frac{2}{3} A D_{minor} \tag{5}$$

so that one can deduce the equivalent diameter in the ellipsoidal approximation:

$$D_{ellips} = \left(\frac{4 A D_{minor}}{\pi} \right)^{1/3} \tag{6}$$

This equivalent diameter can also be expressed as

$$D_{ellips} = D_{sph}^{2/3} D_{minor}^{1/3} \tag{7}$$

which makes clear the essence of the ellipsoidal approximation: the only difference with respect to the spherical approximation is to use D_{minor} instead of D_{sph} for the out-of-plane dimension. Since by definition we necessarily have $D_{minor} \leq D_{sph}$ then $D_{ellips} \leq D_{sph}$ (they can only be equal if the projected area is a perfect disk).

Fig. 1 displays an example of image analysis (deposited FeRh clusters on an amorphous carbon film) with the projected area of the particles (Fig. 1b) and the equivalent ellipses (Fig. 1c) corresponding to an original TEM image (Fig. 1a). The particle size distribution deduced from many such images is given in Fig. 1d, where we clearly see the difference between the spherical and ellipsoidal approximation.

2.3. Grain approximation

Because complex particle shapes may come from the existence of several "grains", with potentially a partial coalescence (see below), one can consider another very basic approximation that we shall call the "grain approximation". Note that tortuous/ramified shapes do not correspond to equilibrium conditions and are thus the result of the particle formation process which can occur by aggregation in gas or liquid phase, or even on the surface (through cluster diffusion) [13,17,69,82,86–90].

In the present approximation, we will imagine the most simple scenario where particles are formed by individual spherical grains of the same size (diameter d_{grain}), touching each-other without any coalescence (like beads). Contrary to complex shaped soot particles (see for instance [6,12,46]) we restrict our model to particles made of a limited number of grains, all lying on the surface. With this assumption, the projected area is necessary a multiple of the single grain area:

$$A = n \frac{\pi}{4} d_{grain}^2 \tag{8}$$

with n integer. The corresponding volume would then be

$$V_{grain} = n \frac{\pi}{6} d_{grain}^3 = \frac{2}{3} A d_{grain} \tag{9}$$

This shows that with this approximation, the out-of-plane dimension is not D_{sph} but d_{grain}. One can also directly see that since $d_{grain} \leq D_{sph}$, the volume and consequently the equivalent diameter will always be lower than that of the spherical approximation. Moreover, the spherical approximation would simply correspond to impose $n = 1$ so that once again, the grain approximation appears as an extension that encompasses the usual spherical approximation. It must then be more powerful. The question that remains is how to determine the n value for a given particle? For the moment, we will circumvent this question by using the perimeter P of the particle, which is simply in this grain model $P = n\pi d_{grain}$. By using the ratio between the projected area and the perimeter, which are both proportional to the number of grains n, we can then write:

$$d_{grain} = \frac{4A}{P} \tag{10}$$

Thus, one can always calculate a value of d_{grain} (as we can always calculate a D_{sph} value) that may or may not be relevant for the particle size analysis. If the grain approximation is adapted to the real experimental situation, and we will discuss later how it can be tested, it will be a sound choice to consider d_{grain} for the out-of-plane dimension. For a spherical particle, the d_{grain} value defined as above is simply equal to the particle diameter D. Therefore, as already explained, the grain approximation is more robust than the spherical approximation since the later appears as a special case of the more general situation (where n can differ from 1).

The particle volume can be written as $V_{grain} = \frac{8A^2}{3P}$ so that the equivalent diameter of a particle is defined by

$$D_{grain} = \left(\frac{16 A^2}{\pi P} \right)^{1/3} = D_{sph}^{2/3} d_{grain}^{1/3} \tag{11}$$

This expression is similar to the one established within the ellipsoidal approximation where we had D_{minor} instead of d_{grain}. This underlines the difference between the three approximations that we have presented up to now. They only differ by the value used for the out-of-plane dimension: D_{sph}, D_{minor} or d_{grain} respectively for the spherical, the ellipsoidal or grain approximation. In the following, as a variable naming convention, we will use lower case d for the out-of-plane dimensions and upper case D for the in-plane or equivalent diameters of different approximations. Note that a table with the list of variables and their meaning is given in Appendix A (see Table A.1).

2.4. Circularity, roundness and comparison of the different approximations

In the definition of the grain diameter, we have used the particle perimeter P. This is an important information when we analyze the shape of a particle. We postpone to Section 4 the discussion on the practical evaluation of the perimeter from a pixelated 2D image, which is not as simple as it may seem. Here we assume that, just as for the projected area A, we have a reliable way to measure the perimeter P. A specially important dimensionless parameter is defined as the *circularity* C [35,37,41–43,75,82,91]:

$$C = \frac{4\pi A}{P^2} \tag{12}$$

It varies between 0 and 1, and can only reach 1 for a perfect disk. It is important to keep in mind that there are many ways to have a particle with a given circularity (except for $C = 1$), for instance having a surface "roughness", ramifications, or an elongated shape will reduce C. While a given shape corresponds to a given C value, the opposite is not true: a shape cannot be fully characterized just from its circularity! It is just a single (useful) parameter, it is therefore logical that it is not sufficient to describe a 2D shape (except for a perfect disk).

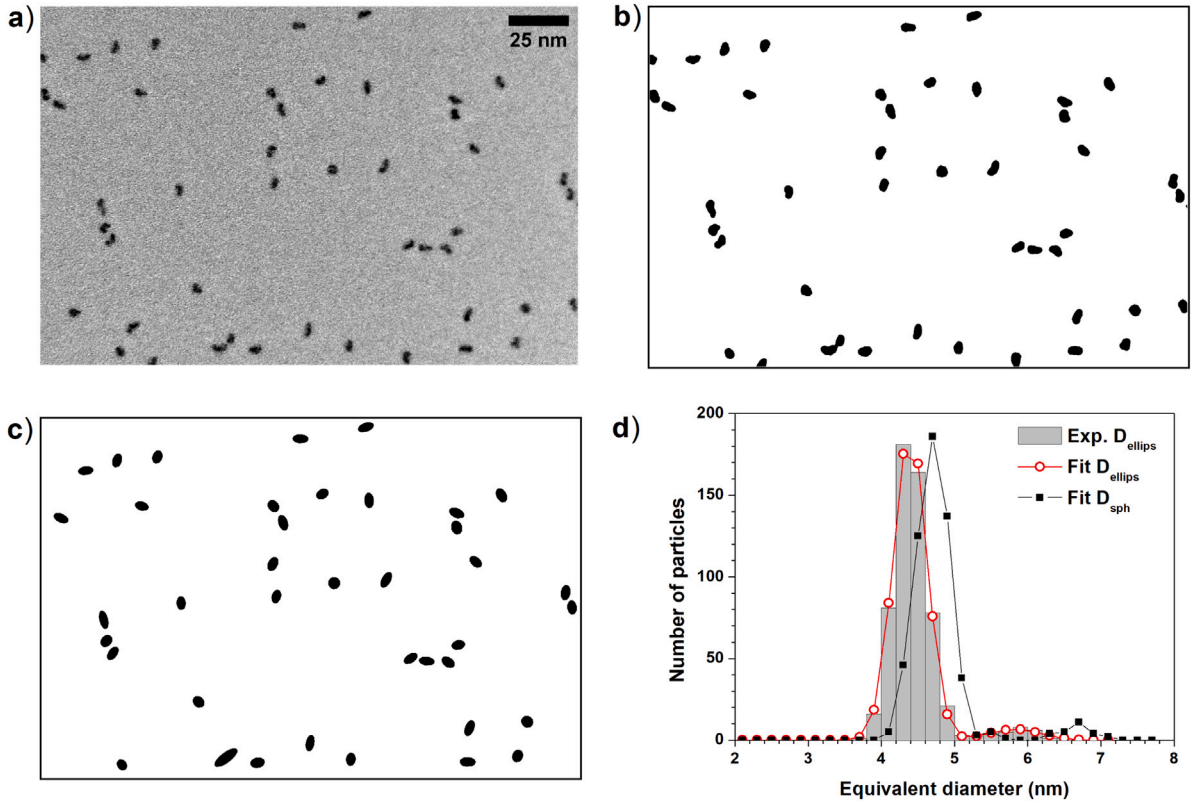

Fig. 1. Transmission electron microscopy (TEM) image of FeRh particles on an amorphous carbon film (a) with the corresponding projected areas (b) (binary image obtained by filtering and thresholding of the gray level image) and equivalent ellipses (c) used to compute the particle size in the spherical or ellipsoidal approximation. By using many such images, one finally obtain the particle size distribution (d): the experimental histogram can be fitted using a bimodal distribution made of two Gaussians (the incident particles, called monomers, and the dimers formed by two incident particles). The spherical approximation would provide a significantly higher equivalent diameter than the ellipsoidal approximation (incident particle size centered on 4.70 nm instead of 4.39 nm).

Interestingly, the circularity can be used to relate d_{grain} and D_{sph}. We indeed can note that

$$\frac{d_{grain}}{D_{sph}} = \sqrt{\frac{4\pi A}{P^2}} = \sqrt{C} \tag{13}$$

and the equivalent diameter of the grain approximation is consequently

$$D_{grain} = C^{1/6} D_{sph} \tag{14}$$

The circularity is thus the relevant parameter to go from the spherical approximation to the grain approximation (once again, for a perfect disk, $C = 1$ and the two expressions are the same).

Another shape descriptor, often provided by imaging softwares when analyzing particles, is the *roundness* r [35,36,39,41,43,72]. This dimensionless parameter, also varying between 0 and 1, is related to the equivalent ellipse discussed above, and is defined by

$$r = \frac{4A}{\pi D_{major}^2} = \frac{D_{minor}}{D_{major}} = \frac{1}{\gamma} \tag{15}$$

where γ is the *aspect ratio* of the equivalent ellipse, i.e. $\gamma = D_{major}/D_{minor} \geq 1$. Note however that, contrary to the circularity, there are plenty of shapes that corresponds to $r = 1$ (or equivalently to $\gamma = 1$). Because the equivalent ellipse is related to the inertia matrix of a particle, r can be equal to 1 if the particle shape is symmetrical enough (for instance with a star shape). While a perfect disk will correspond to $r = 1$, the opposite is not true and in particular, one can have shapes with $r = 1$ and a circularity C far from unity (on the contrary, if C approaches 1 then r is necessarily getting close to 1). This shows that *roundness* and *circularity* are not sensitive in a same way to a deviation from a spherical shape (or disk in 2D). The two parameters are convenient and of interest to analyze the shape of particles.

From the previous discussion on the ellipsoidal approximation, one can note that

$$\frac{D_{minor}}{D_{sph}} = \sqrt{r} \tag{16}$$

and for the equivalent diameter we have

$$D_{ellips} = r^{1/6} D_{sph} \tag{17}$$

Remarkably, this is reminiscent of the relation established for the grain approximation, where instead of the circularity here it is the roundness r which appears as the relevant parameter to go from the spherical approximation to the ellipsoidal approximation. For a perfect disk, of course we have at the same time $C = 1$ and $r = 1$ and all the approximations are equivalent.

If we want to compare the grain and ellipsoidal approximation, we can write

$$\frac{d_{grain}}{D_{minor}} = \sqrt{\frac{C}{r}} \tag{18}$$

for the out-of-plane dimension, and

$$\frac{D_{grain}}{D_{ellips}} = \left(\frac{C}{r}\right)^{1/6} \tag{19}$$

for the equivalent diameter.

If the particles display elliptical projected areas, then there is a one to one relation between the circularity and the roundness (see Fig. 2). Using approximated analytical formula for the perimeter P (which involves elliptic integral or infinite series to get an exact value), we can for instance write, using the quite simple and efficient formula

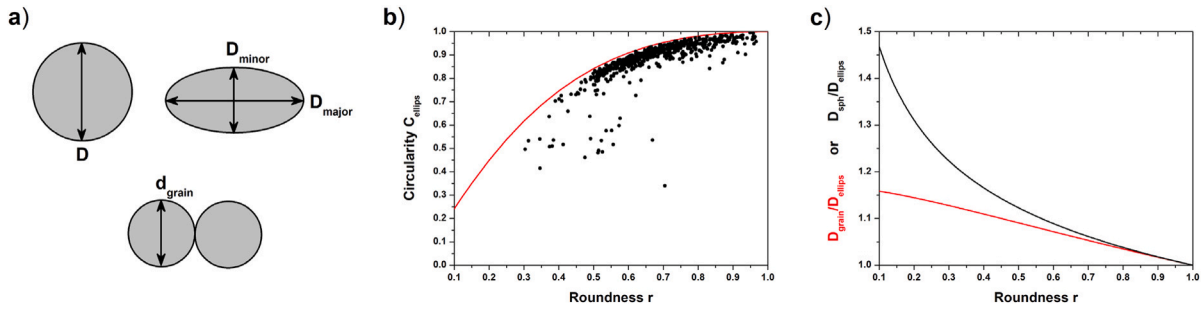

Fig. 2. (a) Projected area for the different hypotheses considered in the text: spherical or ellipsoidal particles, or a particle made of touching grains. (b) Red curve: evolution of the circularity for an ellipse (calculated here with the Muir approximation, Eq. (20)), as a function of the roundness r. Black dots correspond to the distribution of C vs r experimentally measured for the particles corresponding to Fig. 1, showing a good agreement with what is expected for ellipses (except for a few particles with low circularity). (c) Ratio D_{grain}/D_{ellips} or D_{sph}/D_{ellips} calculated for an ellipsoidal particle of different roundness parameter.

proposed by Muir [92,93] ($P \simeq \pi \left[(D_{major}^x + D_{minor}^x)/2\right]^{1/x}$ with $x = 3/2$):

$$C_{ellips} = r\left(\frac{2}{1+r^{3/2}}\right)^{4/3} \tag{20}$$

where we have noted C_{ellips} for the circularity, to emphasize that this is not true in any case but only for an ellipse (this also appears as an upper bound of C vs. r relation in general).

Since for an ellipse C_{ellips} is larger than the roundness r, the parameter d_{grain} is always larger than D_{minor} and thus the grain equivalent diameter D_{grain} will be larger than the ellipsoidal equivalent diameter D_{ellips}, if particles have projected areas close to true ellipses. As shown in Fig. 2, the evolution of the ratio D_{grain}/D_{ellips} as a function of r is very close to a simple straight line. Using the grain approximation for particles that are in fact ellipsoidal would result however in a moderate overestimation of their size (lower than 15% as long as $r > 0.2$, i.e. for particles with an aspect ratio lower than 5). Nevertheless, the error would be even larger if we use the spherical equivalent diameter D_{sph}. This shows that the grain approximation not only encompasses the spherical approximation, but it is still a better choice even in the case of particles having an ellipsoidal shape. Anyway, in such a case, that can be detected by the eyes or with a numerical analysis (for instance looking at the variation of C vs. r, which follows a known curve for perfect ellipses), the ellipsoidal approximation would of course be the wisest choice. On the contrary, one may wonder how bad it would be to use the ellipsoidal expression in the case of particles really corresponding to several identical grains. Since such particles (with a perfectly defined d_{grain}) may adopt different shapes, depending on how the grain are disposed (linear chain, compact island, branched shapes...), the very same D_{grain} value can correspond to completely different roundness parameters. Quantifying the error of using D_{ellips} instead of D_{grain} is not possible, but in any case it would always be better (or identical, for particles with $r = 1$) than the simple spherical approximation.

A convenient way to test the validity of the grain approximation, for a given experimental assembly of particles, is to plot the projected area A of each particle as a function of its perimeter P. Indeed, in the case of a well-defined value of d_{grain}, the relation between A and P will be linear (see Eq. (10)) [94]. The situation will clearly differ from one where the particles are nearly spherical, because in this case the circularity remains close to 1 and the projected area varies as P^2 (for a disk, we simply have $A = \frac{P^2}{4\pi}$). In the case of ellipsoidal particles of fixed roundness, the variation of A vs. P is still quadratic, but in the general case we can write

$$A = \frac{P^2}{4\pi} C_{ellips}(r) \tag{21}$$

the expression of the circularity C_{ellips} as a function of the roundness r being approximately given by Eq. (20) (from Muir analytical expression given above for the perimeter). In an assembly made of ellipsoidal particles with a distribution of r parameter, the resulting evolution of A vs. P^2 will not be a simple straight line: depending on the dispersion of roundness it can still be close to a pure P^2 variation (since C_{ellips} evolves rather slowly with r: for instance it remains over 0.8 for $r > 0.5$) or on the contrary it can display a quite large scattering. In such a case, as mentioned above, a plot of C vs. r for the ensemble of particles is a good way to see if the measurements are close to the theoretical curve $C_{ellips}(r)$, and thus if the use of the ellipsoidal approximation is relevant (i.e. particle size given by the D_{ellips} equivalent diameter).

To evaluate if the spherical approximation is a sound choice or not, one may also look at the circularity value among the particles in the assembly, as they should remain close enough to 1. These considerations emphasize the crucial role of the circularity parameter in the analysis of particle sizes. This implies that the perimeter of each particle must be evaluated with a special care in order to get reliable values. This question will be addressed further (see Section 4). To conclude this section, let us insist on the fact that the three equivalent diameters D_{sph}, D_{ellips} and D_{grain} reach the same value when particles are spherical (more precisely, when the projected area are disks). A comparison between these 3 quantities for a given assembly therefore provides an indication of how far we are from the perfect sphere situation. If the 3 equivalent sizes are nearly identical, the obtained value can be trusted, while if they significantly differ, for sure one must not use the spherical approximation.

3. Partial coalescence model

The grain approximation presented above, with the use of the d_{grain} dimension that can be easily calculated, is a first attempt (to our knowledge) to simply take into account the circularity $C \neq 1$ of particles to better evaluate their equivalent diameter. It appears as a correction to the widely used spherical approximation, with some kind of rescaling through the use of the circularity (see Eq. (14)). However, even if this approximation is always better than the spherical approximation, it may be quite unrealistic. Indeed, particles of complex shapes rarely look like a necklace of touching spherical grains. The existence of an ultimately thin "neck" (point contact between two grains) is something which is definitely not favorable, and if atoms can diffuse, the contact region will evolve with time in order to increase the neck lateral size [88,95–99]. In the following, we would like to extend the grain approximation to a more realistic situation where a partial coalescence can occur. It must be noted that a full coalescence, leading to equilibrium, would in general result in a circular projected area so that the spherical approximation is then adapted [100].

We can parameterize the degree of coalescence by the ratio of the overlapping distance h between two spheres with the spherical grain radius R_g (see Fig. 3). The dimensionless *coalescence parameter* $x = h/R_g$ can thus vary from 0 for no coalescence at all (point contact between grains) to 1 for a full coalescence (single sphere). Such a

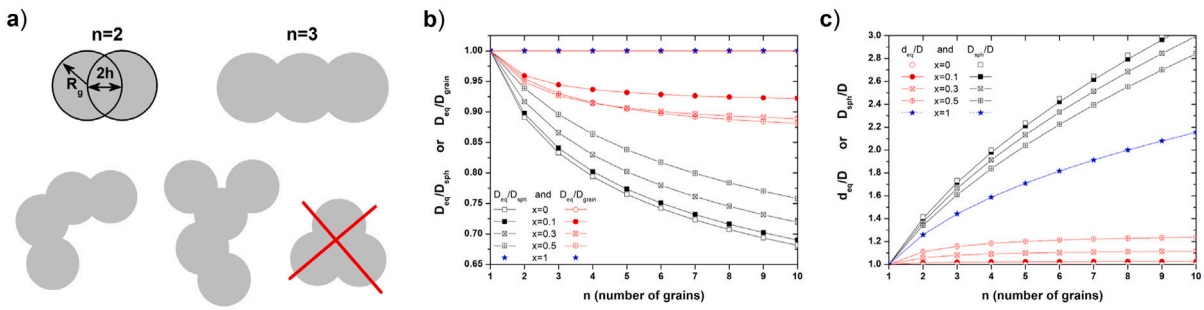

Fig. 3. (a) Illustration of the partial coalescence model, with a particle made of two grains ($n = 2$) i.e. 2 overlapping spheres with a *coalescence parameter* $x = h/R_g$. Particles with a larger number of grains are constructed in the same way, with a linear configuration ($n = 3$ is shown as an example), but as long as x is not too large, the corresponding volume, projected area and perimeter would be the same for n-mers with more complicated (and thus more realistic) arrangements of the grains, as shown here with a tetramer and pentamer. However, the model will not consider particles such as the crossed out one. (b) Ratio D_{eq}/D_{sph} and D_{eq}/D_{grain} calculated for various degrees of coalescence ($x = 0.1$, 0.3, and 0.5, in addition to $x = 0$ and $x = 1$). While the spherical approximation can strongly overestimate the correct equivalent diameter, the grain approximation (i.e. constructed for a situation without any coalescence) provides a quite good estimation (relative error around 10% in the case shown here) even for a coalescence parameter as large as $x = 0.5$. In the limit $x \to 1$, (total coalescence) as expected the two models give the same value. (c) Evolution of the out-of-plane dimension d_{eq} (normalized by the monomer diameter) with the number of grains in the particle, for different degrees of coalescence. It does not vary a lot, even when the coalescence is significant. The value D_{sph} of the spherical approximation is shown for comparison: it strongly overestimates the correct value (except when $x \to 1$).

parameter is commonly used in the context of soot characterization (i.e. particles which are agglomerates of many primary grains), where it is called the "overlap parameter" [12,65,101–104]. We will suppose that x has a fixed value for a given assembly of particles (to complexify the model, one may envisage a variation of x with the particle size for instance). Particles can be made of an increasing number n of grains, all partially coalesced in a same way: monomers for $n = 1$, dimers for $n = 2$, trimers for $n = 3$, etc. (see Fig. 3a). For the general case, a particle is thus a n-mer with an integer value n which is a priori not known [105]. It is possible, within the present model, that the incident particles are in fact themselves made of several grains (in such a case, only a particular sequence of n-mers would then be obtained, corresponding to multiples of the incident size). For strong coalescence, let say typically $x \geq 0.5$, the resulting particles (except maybe for n-mers of large n) have shapes that tend to look like ellipsoids, so that the ellipsoidal approximation should become acceptable. We are thus particularly interested in the case of moderate to low coalescence, x having a small but finite value, which allows us to improve the crude "grain approximation" seen before.

3.1. Analytical expressions

For simplicity, we will only consider n-mers corresponding to "linear" chains of grains (the particles may have more tortuous shapes, but except the final grains on the border, each grain is supposed to overlap with two neighboring grains). It may seem far from a realistic situation but we have to keep in mind that other usual approximation are worse! We also implicitly assume that as n increases, the number of n-mers in the assembly is getting lower [70] (i.e. the dimers are more abundant than trimers, which are themselves more abundant than tetramers etc., so that no long chains are found in the experimental particle assembly). The experimental relevance of this partial coalescence model will be illustrated later.

Simple geometry allows us to write, for a given coalescence degree x and a number n of grains, the projected area A_n, the perimeter P_n and the volume V_n of a particle. If we call D the initial diameter of a spherical grain, before coalescence, then the volume of a n-mer is by definition (this is true for any x value, because coalescence does not change the total volume of matter):

$$V_n = n\frac{\pi D^3}{6} \tag{22}$$

The grain radius R_g of the finally overlapping spheres is different from $D/2$, and its value will depend both on x and n (of course, we simply have $R_g = D/2$ for $n = 1$). Noting $V_0 = \frac{4}{3}\pi R_g^3$, $A_0 = \pi R_g^2$ and $P_0 = 2\pi R_g$, helps us to express the quantities V_n, A_n and P_n. Let us emphasize that V_0, A_0 and P_0 are not fixed values but functions of n and x, through the quantity $R_g(n, x)$. For a dimer particle we can write for instance:

$$V_2(x) = 2V_0\left[1 - \frac{x^2(3-x)}{4}\right] = 2V_0\epsilon_V(x) \tag{23}$$

$$A_2(x) = 2A_0\left[1 - \frac{\mathrm{acos}(1-x) - (1-x)\sqrt{1-(1-x)^2}}{\pi}\right] = 2A_0\epsilon_A(x) \tag{24}$$

$$P_2(x) = 2P_0\left[1 - \frac{\mathrm{acos}(1-x)}{\pi}\right] = 2P_0\epsilon_P(x) \tag{25}$$

where we have introduced the three functions ϵ_V, ϵ_A and ϵ_P which vary from 1 (for $x = 0$) to 1/2 (for $x = 1$). Doing the same for a n-mer, we can write:

$$V_n(x) = nV_0\epsilon_{V,n}(x) \tag{26}$$

$$A_n(x) = nA_0\epsilon_{A,n}(x) \tag{27}$$

$$P_n(x) = nP_0\epsilon_{P,n}(x) \tag{28}$$

where the three ϵ functions vary between 1 (for $x = 0$) and $1/n$ (for $x = 1$) and correspond respectively to

$$\epsilon_{V,n}(x) = 1 - \frac{n-1}{2n}x^2(3-x) \tag{29}$$

$$\epsilon_{A,n}(x) = 1 - \frac{2(n-1)}{n\pi}\left[\mathrm{acos}(1-x) - (1-x)\sqrt{1-(1-x)^2}\right] \tag{30}$$

$$\epsilon_{P,n}(x) = 1 - \frac{2(n-1)}{n\pi}\mathrm{acos}(1-x) \tag{31}$$

These functions can then be used to determine the apparent grain radius (simply $R_g = D/2$ for $n = 1$)

$$R_g(n, x) = \frac{D}{2}\epsilon_{V,n}(x)^{-1/3} \tag{32}$$

and, combined together, can provide the ratio between the equivalent diameter D_{eq} (the one that would correspond to the exact volume, see Eq. (1)) and D_{grain} or D_{sph} (respectively the grain approximation and spherical approximation equivalent diameter, introduced in Section 2):

$$\frac{D_{eq}}{D_{grain}} = \epsilon_{P,n}(x)^{1/3}\epsilon_{V,n}(x)^{1/3}\epsilon_{A,n}(x)^{-2/3} \tag{33}$$

$$\frac{D_{eq}}{D_{sph}} = n^{-1/6}\epsilon_{V,n}(x)^{1/3}\epsilon_{A,n}(x)^{-1/2} \tag{34}$$

The evolution of these ratios is shown in Fig. 3b, for different x values and up to $n = 10$. It is clear that D_{grain} is always closer to the true D_{eq} value than D_{sph}, and that it is a quite good estimation of the correct equivalent particle diameter (even if a better approximation can be

proposed, see further). The circularity $C_n(x)$ (written this way since it depends on x and n) can also be expressed by:

$$C_n(x) = \frac{4\pi A_n(x)}{P_n(x)^2} = \frac{\epsilon_{A,n}(x)}{n\epsilon_{P,n}(x)^2} \tag{35}$$

and the out-of-plane dimension in the grain approximation is

$$d_{grain} = D\frac{\epsilon_{A,n}(x)}{\epsilon_{P,n}(x)\epsilon_{V,n}(x)^{1/3}} \tag{36}$$

3.2. Simple approximation for the out-of-plane dimension

The out-of-plane dimension, which relates the particle volume to its projected area, is given by

$$d_{eq} = \frac{3V_n}{2A_n} = D\frac{\epsilon_{V,n}^{2/3}}{\epsilon_{A,n}} \tag{37}$$

where the x dependence is not explicitly written. Note, that d_{eq} is also the dimension allowing us to relate the exact equivalent diameter to the spherical diameter, through the equation:

$$D_{eq} = D_{sph}^{2/3} d_{eq}^{1/3} \tag{38}$$

It is interesting to see that this dimension (which is by definition equal to the monomer diameter D for $n = 1$) does not evolve much with the number of grains in a particle (see Fig. 3c). While this is expected for a small x value, it is not so intuitive for larger degrees of coalescence (of course, for $x \to 1$ it is not true any more). Notably, for a significant coalescence parameter $x = 0.3$, compared to monomers d_{eq} is only around $\simeq 10\%$ larger for trimers and less than 15% larger for 10-mers. One may compare this to the value we would deduce by using the usual spherical approximation. In such a case, one finds

$$\frac{D_{sph}}{D} = \frac{n^{1/2}\epsilon_{A,n}^{1/2}}{\epsilon_{V,n}^{1/3}} \tag{39}$$

which would erroneously lead to a factor about 1.6 for trimers and 3 for 10-mers, again for a $x = 0.3$ coalescence parameter.

One can compare the correct out-of-plane dimension d_{eq} with D_{sph} on one hand and with d_{grain} on the other hand. From the expression established above, we can write

$$\frac{d_{eq}}{D_{sph}} = \frac{\epsilon_{V,n}}{n^{1/2}\epsilon_{A,n}^{3/2}} \quad \text{and} \quad \frac{d_{eq}}{d_{grain}} = \frac{\epsilon_{P,n}\epsilon_{V,n}}{\epsilon_{A,n}^2} \tag{40}$$

and the evolution of these ratios is shown in Fig. 4a as a function of the coalescence parameter x, for some multimers up to $n = 10$. One can see again that the grain approximation is a better choice than the spherical approximation, on the entire range of coalescence degree. d_{grain} is not so far from the correct (equivalent) out-of-plane dimension, the worst case being for quite strong coalescence (typically for x between 0.5 and 0.7). d_{grain} will then be used as a starting point to find a simple expression of the out-of-plane dimension, even closer to the true value. Since the value of n and x is a priori not known for a given observed particle, we would like to use a measured quantity, namely the particle circularity C, to parameterize the estimation of the out-of-plane dimension. In Fig. 4b, we show the same kind of curves but as a function of the circularity instead of x. Indeed, for a given family of particles (n-mers), we can plot a curve d_{eq}/d_{grain} vs $C_n(x)$. Then, for a given x (which is supposed to be the same for all the n-mers), we can visualize the evolution of the ratio d_{eq}/d_{grain} with the circularity (for $x = 0.1$, 0.3 and 0.5 in Fig. 4b for instance). Note that for $n = 1$, we have $d_{eq} = D = d_{grain}$, while for $C = 1$ of course d_{eq} is also equal to d_{grain}. For large values of n, the ratio d_{eq}/d_{grain} displays a quasi-linear variation with the circularity, with a limit value at $C \to 0$ decreasing with x. We can propose the following simple analytical expression to approach the true $d_{eq}(C)$ curve:

$$d_\alpha = d_{grain}[1 - (1-\alpha)\sqrt{1-C}] \tag{41}$$

This equation ensures that $d_{eq} = d_{grain}$ for $C = 1$, and has only a single adjustable parameter $\alpha(x)$ which can be chosen to provide the best approximation for a given coalescence degree x (note that α corresponds to the limit of d_α/d_{grain} at $C \to 0$, i.e. at $n \to \infty$). We find that a good choice is to force the ratio d_α/d_{grain} to coincide with the true d_{eq}/d_{grain} ratio at $n = 5$ (which corresponds somehow to a middle-ranged circularity): this is completely arbitrary but it should give precise results on a extended range of n-mer particles. However, since the experimental value of x is unknown, one has to keep in mind that the α value in the d_α expression is an adjustable parameter (but in a quite limited range, let say between 0.55 and 0.75, see Fig. 1 in supplementary information [106]). Let us also emphasize that for almost perfect coalescence (x values approaching 1), the magnitude of α does almost not play any role since the circularity will be limited to values close to 1. On the contrary, in the limit of no coalescence (i.e. just touching spheres, as in the grain approximation), $d_{eq} \to d_{grain}$ and thus, for $x \to 0$ the coefficient α must go to 1. We will call in the following the *alpha approximation*, the use of the above expression of d_α (Eq. (41)) for the out-of-plane dimension. Within this approximation, supposed to be best adapted in the case of a partial coalescence, an equivalent particle size D_α (i.e. the spherical equivalent diameter of the alpha approximation) can be calculated:

$$\frac{\pi D_\alpha^3}{6} = \frac{2}{3}Ad_\alpha \quad \text{so that} \quad D_\alpha = D_{sph}^{2/3} d_\alpha^{1/3} \tag{42}$$

This quantity can be eventually compared to the theoretical D_{eq} value, via the ratio D_{eq}/D_α (which is also equal to $(d_{eq}/d_\alpha)^{1/3}$). This is what is shown in Fig. 4c, on the entire range of coalescence parameter (x from 0 to 1) for some families of n-mers up to $n = 10$. It is remarkable that up to $n = 5$ the particle size deduced with the alpha approximation is deviating from the true value by less than 1% (the results are even more precise in the range of x particularly relevant, i.e. around 0.3–0.5). Even for long chains of grains such as particles corresponding to $n = 10$, the error in the equivalent diameter is still quite negligible (slightly over 1% when $x \simeq 0.7$). To realize the gain offered by the present approximation, with respect to the crude spherical approximation, one can compare this ratio to the data of Fig. 3b. This demonstrates how partially coalesced particles can be analyzed in a much more powerful and reliable way than with the usual spherical approximation. One can write in a quite condensed way the expression of the equivalent diameter in the frame of this alpha approximation:

$$D_{eq} \simeq D_\alpha = D_{sph}\, C^{1/6}\left[1 - (1-\alpha)\sqrt{1-C}\right]^{1/3} \tag{43}$$

which can also be written as a function of the perimeter P and circularity (which of course depends on the area A)

$$D_{eq} \simeq D_\alpha = \frac{P}{\pi}C^{2/3}\left[1 - (1-\alpha)\sqrt{1-C}\right]^{1/3} \tag{44}$$

3.3. Area vs perimeter evolution

We have seen in Section 2 that, if the grain approximation is valid, the projected area A varies linearly with the perimeter P. To what extent will it remain the case when a partial coalescence occurs? In the extreme case of full coalescence ($x = 1$) we recover the spherical limit and A follows a P^2 evolution. Since by definition we have $d_{grain} = 4A/P$, having a quasi-linear relation between A and P is equivalent to have a well-defined value of d_{grain} for all the particles in an assembly, i.e. for all the n-mers (limited to a reasonable n value) with a fixed coalescence degree. Here again, we know that this will not be true in the limit of an almost perfect coalescence ($x \to 1$).

In Fig. 5a, we plot the evolution of d_{grain} with the number of grains in the particles, for different values of x. Except at low x, one can hardly tell that the value is constant for all n-mers. On the contrary, as already noticed on Fig. 3c, the equivalent out-of-plane diameter d_{eq} remains well-defined, up to quite large values of n, even with a significant coalescence. Since d_α was shown to be a very good approximation of the true d_{eq} size, it is no surprise that it displays a similar behavior: it remains almost constant for all n-mers in a particle assembly, with

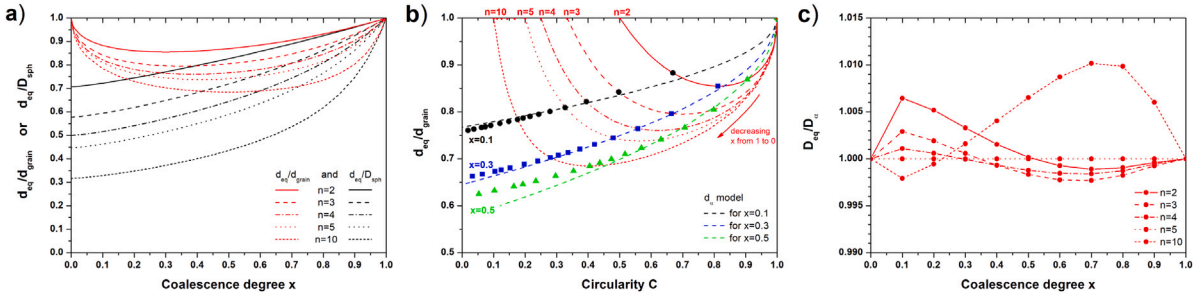

Fig. 4. (a) Evolution of d_{eq}/d_{grain} and d_{eq}/D_{sph} with the coalescence degree x, for different n-mers (n = 2, 3, 4, 5 and 10). The correct out-of-plane dimension can be highly different from the spherical approximation one, especially for low x values and large n. On the contrary, the grain approximation gives the correct value for $x = 0$ and $x = 1$ and does not deviate so much from d_{eq}. (b) Same d_{eq}/d_{grain} curves, for a given n as in (a), but plotted as a function of the circularity C, which itself directly depends on x. The ratios calculated for n = 1-10 and larger values (n = 12, 15, 20, 25, 30, 50, 100) are also shown as scattered points, for 3 selected values of the coalescence degree (x = 0.1, 0.3 and 0.5), together with the analytical curve (dashed curves) corresponding to the *alpha approximation* (see text). (c) Equivalent diameter ratio D_{eq}/D_{α}, for different n-mers (n = 2, 3, 4, 5 and 10), as a function of the coalescence degree x. The precision of the alpha approximation can be appreciated, especially by comparison with the spherical approximation as shown with the data of Fig. 3b.

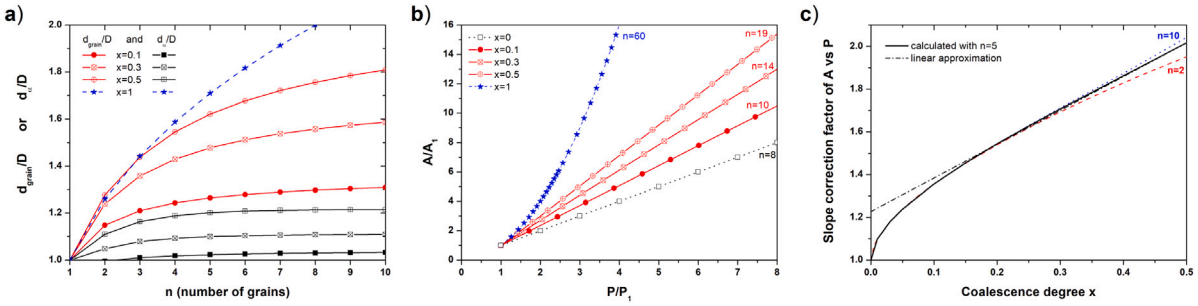

Fig. 5. (a) Variation of the ratio d_{grain}/D and d_{α}/D with n, for different degrees of coalescence x. (b) Evolution of the projected area A (normalized by the area A_1 of monomers) with respect to the perimeter P (also normalized by the perimeter P_1 of monomers). Even with a coalescence parameter x as large as 0.5, the variation appears quasi linear, much different from the parabolic evolution corresponding to the spherical case (full coalescence, i.e. $x = 1$). The maximum n value in the graph is indicated for each curve. (c) Variation of the A vs P slope correction factor (with respect to $D/4$, which corresponds to $x = 0$, see text) with the coalescence degree x. The black curve is calculated with $n = 5$ but note that considering $n = 2$ or $n = 10$ does almost give the same value.

variations less than 10% for $x = 0.3$, or 20% for $x = 0.5$. Such a variation with respect to the monomer diameter must be often smaller or comparable to the natural size dispersion met in a real sample. This means that a narrow grain size distribution will also correspond to a quite narrow effective out-of-plane dimension (as expressed with d_{α}) as long as the partial coalescence model is relevant.

Interestingly, despite the evolution of d_{grain} with n, the partial coalescence signature is clearly visible on a A vs P plot: the evolution remains linear, as for the ideal grain model (i.e. $x = 0$), even for a coalescence degree as large as $x = 0.5$. Indeed, from the expression established above, we can write

$$\frac{A_n}{A_1} = \frac{n\epsilon_{A,n}}{\epsilon_{V,n}^{2/3}} \quad \text{and} \quad \frac{P_n}{P_1} = \frac{n\epsilon_{P,n}}{\epsilon_{V,n}^{1/3}} \tag{45}$$

where $P_1 = \pi D$ and $A_1 = \pi D^2/4$ are respectively the perimeter and projected area of monomers. The calculated values are reported in Fig. 5b, for different values of x. The linear A vs P regime, as opposed to the parabolic evolution met for spherical or ellipsoidal particles, is thus a signature to look at in order to experimentally detect that we are in a partial coalescence situation (see further for experimental illustrations). It may be particularly convenient to use a log–log plot of A vs P to make the distinction between a linear and a quadratic variation.

The linear behavior of A vs P curves can also be used to experimentally infer the grain size D (i.e. the diameter of a single grain, called a monomer) constituting the particles. From the previous expressions, we can express the slope as

$$\frac{A_n - A_1}{P_n - P_1} = \frac{D}{4}\left(\frac{n\epsilon_{A,n}\epsilon_{V,n}^{-2/3} - 1}{n\epsilon_{P,n}\epsilon_{V,n}^{-1/3} - 1}\right) \tag{46}$$

which shows that the slope is close to $D/4$, corrected by a factor that must be almost constant with n, but which varies with the degree of coalescence x (keep in mind that the x dependence of the ϵ functions is implicit). The correction factor is shown in Fig. 5c, for x between 0.1 and 0.5 it varies almost linearly with a typical value between 1.3 and 2. In this relevant range for the partial coalescence model, the slope correction factor is approximately equal to $1.222 + 1.58x$. Let us emphasize that a plot of A vs P in an assembly of particles will thus be a powerful technique: (i) to detect that the grain approximation with partial coalescence is adapted; (ii) to have an idea of the typical grain size D constituting the particles. Moreover, it should be kept in mind that the smallest particles (deposited monomers, i.e. individual incident particles on the surface) may in fact be made of several initial grains (of size D): if they correspond to n_{min} grains, only n-mers which are multiples of n_{min} will be observed on the A vs P curve. This will not change the overall slope, so that the individual grain size D can be inferred and subsequently compared to the projected area of the single particles: the value of n_{min} can then be determined, with potentially a signature that it is larger than 1, that could be of interest concerning the formation process of the particles [17,86,89,90].

3.4. Other considerations

Another possible way to detect the validity of the partial coalescence model is to look at the evolution of the circularity C with the inverse

perimeter $1/P$ of each particle. For the grain approximation and as long as x is not too large, C will vary linearly with $1/P$, while it will be constant (or dispersed without any linear pattern) for spherical or ellipsoidal particles. Indeed, as discussed above for an ellipse, C is directly linked to r so that it will be constant for a given r, which is another way to see that the area scales with P^2 in such a case. For very strong coalescence degree (x approaching 1), n-mers tend to have shapes (projected area) which can be approximated by ellipses, so that the particle size distribution determined within the ellipsoidal approximation (or even with the spherical approximation) will merge with that determined with the present partial coalescence model. Anyway, even if it encompasses the spherical approximation, the partial coalescence model (with the approximate d_α determination from A and P of each particle) is relevant as long as a linear trend between A and P is observed. When the evolution is parabolic, the ellipsoidal approximation (which also encompasses the spherical approximation) should be preferred, and one will use the projected area A and the roundness r to compute each particle equivalent size.

As discussed above (and see Fig. 3), D_{grain} (which corresponds to the use of d_{grain} as out-of-plane dimension) is always a better choice than D_{sph} and it is directly defined from the area and perimeter of a particle, i.e. without any arbitrary parameter. The alpha approximation allows us to further improve the particle size determination, provided that the coalescence degree x is known: we can approximate the true equivalent diameter D_{eq} with D_α, to a very high degree of precision when the α constant is correctly chosen. This approximation simply uses the circularity C of each particle to convert the measured d_{grain} to the more precise d_α out-of-plane dimension. Since the circularity directly stems from the value of A and P, in fact no additional quantity is required. One may wonder what value of x (and consequently of α) must be preferred when analyzing a real assembly of particles where the coalescence degree is a priori unknown (if such a quantity makes sense). We can notice that the alpha approximation is convenient since the best α value does not depend so much on the magnitude of x (see Fig. 1 of supplementary information [106]) and something like $\alpha = 0.65$, corresponding to $x \simeq 0.3$ i.e. a moderate coalescence, should be a good choice in most of the situations.

Anyway, there are other means to infer the degree of coalescence from experimental measurements. A simple parameter to look at is the ratio between the projected area of dimers A_2 and that of monomers A_1 [107]: provided the particle density on the surface is large enough, and the individual grain size D not too dispersed, a clear peak of dimers is visible on the projected area histogram [20,70]. From Eq. (43) seen earlier, we can write

$$\frac{A_2}{A_1} = \frac{2\epsilon_{A,2}}{\epsilon_{V,2}^{2/3}} \tag{47}$$

and remarkably, this ratio is almost a perfect straight line between $x = 0.1$ and $x = 1$ (see Fig. 2 of supplementary information [106]). With no coalescence ($x = 0$), dimers are made of two touching grains and $A_2/A_1 = 2$, while for a perfect coalescence ($x = 1$) they form a single disk and $A_2/A_1 = 2^{2/3}$. Therefore, from the measured ratio one can deduce an effective value of the degree of coalescence:

$$x \simeq \frac{2.02 - A_2/A_1}{0.43} \tag{48}$$

Of course, the consistency with the existence (or not) of a linear evolution of A vs P among the entire assembly of particles should be checked. Besides, as shown in Fig. 5, with the correct α in the alpha approximation, the deduced d_α of each n-mer population are almost the same (except for large coalescence degrees), so that a single peak should appear in the out-of-plane dimension histogram (the width will depend on the dispersion of initial grains/monomers). This criterion is a good indication that the out-of-plane dimensions have been correctly evaluated. The consistency should also be verified with the slope of A vs P, which is supposed to be $D/4$ multiplied by a correction factor between 1.3 and 2 (typically it is around 1.7 for $x = 0.3$). The grain size D inferred from the measured slope (and assuming a given x value) should be comparable to the average d_α out-of-plane dimension. Interestingly, since the volume of dimers must be (by definition) twice the volume of monomers, we can deduce the theoretical ratio of out-of-plane dimension from the measured A_2/A_1 ratio. Namely $d_{eq,\mathrm{dimer}}/d_{eq,\mathrm{monomer}} = 2A_1/A_2$ (and more generally, $d_{eq,n-\mathrm{mer}}/d_{eq,\mathrm{monomer}} = nA_1/A_2$), which allows us to know a priori how much the d_{eq} of dimers will be shifted with respect to that of monomers. We find that typically for $x < 0.5$ the relative difference of out-of-plane dimension between monomers and dimers will be less than 10%: except for highly monodispersed monomers, this difference will not produce a separate peak in the histogram (while in the projected area histogram a clear dimer peak can be detected).

One may also wonder how the *height* H of the particles will be related to the other parameters. The height (as it could be measured for instance by AFM/STM or other techniques such as tomography or grazing-incidence small angle X-ray scattering (GISAXS) [16,24,30,58,60,83,108,109]) corresponds to $H = 2R_g$, and is thus a function of n and x (see Eq. (32)). Intuitively, the out-of-plane dimension (constructed to relate the exact volume, to the projected area of the particle) should be nearly equal to H. Precisely, one can establish

$$\frac{H}{d_{eq}} = \frac{\epsilon_{A,n}}{\epsilon_{V,n}} \tag{49}$$

which appears to keep a value close to 1 (see Fig. 3 of supplementary information [106]). Within roughly 10% of error, the quantity d_α which itself is a very good approximation of d_{eq} will then reflect the height of the particles: as long as x is not too large (linear A vs P regime), all n-mers will correspond to a well-defined d_α value (see Fig. 5a) and equivalently to a well-defined height H. When x approaches 1 (total coalescence) the particles becomes spherical and each n-mer corresponds to a different d_{eq} (or equivalently d_α, i.e. one may observe multiple peaks in the distribution of d_α), but we still have $H \simeq d_{eq}$ and indeed each n-mer has a different height.

Let us insist on the fact that all the previous discussions are of practical use only if monomer particles have well-defined sizes (narrow size distribution of the incident particles, and thus of the constitutive grains of the particles: the D relative dispersion must remain low enough to separate the population of monomers from other n-mers in the size histogram). The calculations were made here with a unique D value, which is of course not realistic: in a true nanoparticle assembly, instead of discrete values of the circularity (and A or P) we will observe a continuum, reflecting the size dispersion. The important point, that has a broad implication, is that for an individual particle the measured circularity can be used to evaluate its out-of-plane dimension, in a simple way that allows us to go much beyond the usual spherical approximation.

4. Illustration with some nanoparticles examples

We will now illustrate the previous discussion, and especially the benefits of the approach exposed in Section 3, on real nanoparticle assemblies observed by TEM. As the perimeter P of each particle plays a central role (it is needed to compute the grain diameter $d_{grain} = 4A/P$ and the circularity $C = 4\pi A/P^2$), we start by examining the not-so-trivial problem of its experimental evaluation from digital images.

4.1. Experimental evaluation of the perimeter

Image analysis nowadays relies on computer software using digital (i.e. pixelated) images. Beyond the question of image processing (cleaning steps, thresholding etc.) [28,31,32,37,38,41,77,110–112], once an image consists of perfectly defined particles (black pixels over a white background as in Fig. 1), one may think that it is an easy task to measure the area A and perimeter P of each object. This task is in fact more subtle than it looks, and the question was examined a long time

ago (and is still under investigation) [35,37,113–118]. While for the area one can just count the number of black pixels (or half pixels in case of diagonals), what will lead to a correctly converging value when the image resolution is increasing, the usual way to compute a length from a pixelated/digitized curve may lead to a systematic error even in the limit of an infinite resolution.

From the early days of computer science, the so-called Freeman estimation has been used [113]: it consists in considering a unit length ℓ (pixel dimension) for vertical or horizontal moves on a contour, and a $\sqrt{2}\ell$ length for diagonal moves. This is a very simple, intuitive and convenient way to compute the length of a given line (each pixel has 8 possible neighbors, which explains why the so-called 8-chain code of a contour is used for the length determination). The problem with the Freeman estimation is that it gives the true length only for straight lines which are either horizontal or vertical, or at 45Â°. This estimator is for instance the one implemented in the very complete Particles8 plugin [119] for the ImageJ free software, providing a powerful particle analysis tool with many shape descriptors. However, the calculated perimeter appears to be often overestimated, so that the circularity of particles with almost perfect ellipsoidal or spherical shapes is downshifted compared to the expected theoretical value.

Other estimators have been proposed, which are not more complicated than that of Freeman: one can still use the 8-chain code but with a chosen length for horizontal/vertical moves and diagonals which has been optimized to reduce the root-mean-square error for randomly oriented straight lines [117,120], or for arc of circles [114], or one can also add the so-called *corner count* to obtain a closer value [117]. When the Freeman estimation is used, we observe a systematic overestimation of the perimeter resulting in an artificial downshift of the circularity (as well as d_{grain} and other quantities related to this parameter). This is clearly visible with a sample where particles have almost spherical shapes, like the Pb nanoparticles shown in Fig. 4 of supplementary material [106]. This is why we recommend to use a more precise perimeter calculation, as we have implemented in the (free, with a GNU General Public Licence) java plugin for ImageJ *ParticlesShape.java*, also provided in supplementary material. Note that this plugin provides a better estimation of the area and perimeter of each particle, plus additional shape parameters (equiv. ellipse, circularity, Feret diameter etc.), and the subsequent particle diameter determination is left to the user, simply by using the output data and the framework of his/her choice (spherical approximation, ellipsoidal approximation, alpha approximation with a chosen α value or any other way to exploit the measured parameters).

4.2. Irregular particles: benefits of the partial coalescence approach

In Fig. 6 we show as an example, the analysis of a Co_3Pt nanoparticle assembly (particles have been size-selected and deposited on amorphous carbon for TEM investigations), which is quite diluted: the size histogram reveals a main peak (*monomers*, that can be fitted with a Gaussian) and a small secondary peak (only a few percent of larger particles) corresponding to two incident particles that have come into contact. These *dimers* should thus have an average volume twice the one of the incident particles. The different plots of Fig. 6 indicate that the particles are not too far from the ellipsoidal approximation, but with a roundness dispersed roughly from 0.4 to 1. The A vs P evolution is apparently rather in an intermediate situation, even if a linear trend seems better. From the projected area histogram (not shown), the ratio $\overline{A_2}/\overline{A_1} \simeq 1.977$ would correspond to a coalescence degree $x \simeq 0.1$. From the volume histogram (Fig. 6b) one can deduce the mean equivalent diameter of monomers and dimers, respectively $\overline{D_1}$ and $\overline{D_2}$, and also directly compare the volume ratio $\overline{V_2}/\overline{V_1}$ with the theoretical value of 2. The values are reported in Table 1, where one can see how the spherical approximation is not correct, and how the partial coalescence model (alpha approximation) performs better, providing almost the exact position of the dimer peak. Of course one may think that using an equivalent diameter of 3.7 nm instead of 3.4 nm is not a problem, but we would like to emphasize that it would almost correspond to a 30% overestimation of the particle volume (this can be problematic when a quantity scaling with the volume, for instance the magnetic moment or the magnetic anisotropy, is determined using a given particle size). Without surprise, we can see that the ellipsoidal approximation provides a better result than the spherical approximation (it performs very well for the monomers, but is less adapted to dimers than the alpha approximation). Notably, the out-of-plane dimension (i.e. d_α histogram, not shown) is well defined, with a single peak centered on 2.93 nm, what would thus correspond to the average particle height (particles could then be slightly flattened, since the average *in-plane* diameter is $D_{sph} = 3.70$ nm).

Table 1
Data corresponding to the sample of Fig. 6 (i.e. Co_3Pt nanoparticles deposited on amorphous carbon). The different approximations for the particle size determination are compared: spherical, ellipsoidal, grain and alpha (partial coalescence, here with $\alpha = 0.65$). The comparison is given for the monomer mean diameter $\overline{D_1}$, the dimer mean diameter $\overline{D_2}$ and its deviation from the expected value (that would give a volume of dimers twice that of monomers), as well as the ratio $\overline{V_2}/\overline{V_1}$ which should in principle be equal to 2.

Approximation	Spher.	Ellips.	Grain	Alpha
Monomer equivalent diameter $\overline{D_1}$ (nm)	3.70	3.41	3.58	3.40
Dimer equivalent diameter $\overline{D_2}$ (nm)	5.29	4.60	4.84	4.40
Deviation from theoretical $\overline{D_2}$	16.8%	8.8%	9.2%	3.4%
$\overline{V_2}/\overline{V_1}$ ratio	2.91	2.45	2.47	2.16

Another interesting example is shown in Fig. 7 and the data in Table 2. It corresponds to the same FeRh particles (mass-selected, deposited on amorphous carbon with a high density, so that many dimers and larger n-mers are formed), observed as deposited or after annealing (2 h at 700°C). The rather tortuous shapes become more spherical after annealing, and the A vs P scaling is completely different, going from a linear behavior to a parabolic one. The circularity and roundness also evolve, remaining quite dispersed but close to the theoretical ellipse relation for annealed particles. The equivalent diameter D_α is very different from that of the spherical approximation D_{sph} for the as-deposited particles. On the contrary, after annealing the different equivalent diameters are quite close to each other (even if D_{sph} is still an overestimation of the true size). What is remarkable is that the out-of-plane dimension, as deduced from the d_α histogram (see Fig. 7g), is completely different from the one of D_{sph}: it reduces to a single peak, very well defined (centered on 5 nm). This would thus correspond to the height of the particles, which is almost constant among the particles despite their very different projected area (i.e. in-plane size). Note that it is only with the alpha approximation that we obtain a ratio $\overline{V_2}/\overline{V_1}$ approaching the correct value of 2. This is another indication of the strength of the partial coalescence model developed here. Let us also emphasize the strong error that would be made on the equivalent thickness for as-deposited particles (there is also always a significant uncertainty, explaining why the measured value before and after annealing is not exactly the same): around 21 Å for the spherical approximation instead of 8 Å for the alpha approximation (more than a factor 2). Another striking feature is that the equivalent diameter $\overline{D_1}$ of the alpha approximation, calculated for the as-deposited particles, is in perfect agreement with the particle size after annealing. This is normal since the annealing step only leads to a change of particle shape but conserves the volume of monomers and thus their equivalent diameter. Note that the best choice for the particle determination after annealing is the ellipsoidal approximation (see the very good correspondence with the ellipse theory on Fig. 7d), even if the alpha approximation provides almost the same results. Anyway, we hope that Table 2 makes it clear that there is always a better choice than the crude spherical approximation.

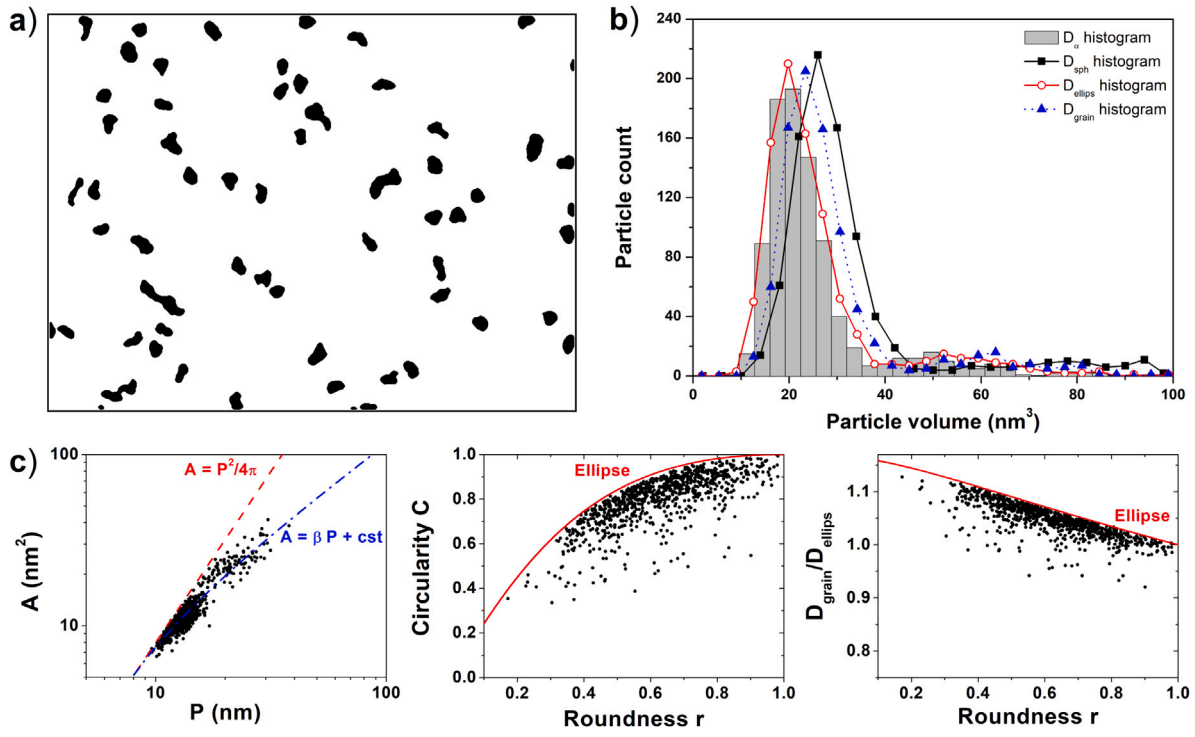

Fig. 6. Example of a nanoparticle assembly (Co_3Pt particles on amorphous carbon) analyzed with the different approximations: spherical, ellipsoidal, grain and alpha (partial coalescence, here with $\alpha = 0.65$). A typical binary image (size 128 nm × 96 nm) is shown in (a), while the volume histograms (calculated with the appropriate out-of-plane dimension of each approximation) are shown in (b). The A vs P evolution (log scale) as well as C and D_{grain}/D_{ellips} vs roundness r for comparison with the ellipse model (red curves) are given in (c).

Table 2
Data corresponding to the samples of Fig. 7 (i.e. the same FeRh nanoparticles deposited on amorphous carbon, before and after annealing). The different approximations for the particle size determination are compared: spherical, ellipsoidal, grain and alpha (partial coalescence, here with $\alpha = 0.65$). The comparison is given for the monomer mean diameter $\overline{D_1}$ (first and most intense peak in the size distribution), the ratio $\overline{V_2}/\overline{V_1}$ of the dimer to monomer volume (calculated with the appropriate out-of-plane dimension of each approximation), and the equivalent thickness e deduced from the total FeRh volume divided by the corresponding area of observation (10 images as the one shown in Fig. 6).

Sample	As deposited				Annealed			
A vs P Evolution	Linear				Parabolic			
Approximation	Spher.	Ellips.	Grain	Alpha	Spher.	Ellips.	Grain	Alpha
Diameter $\overline{D_1}$ (nm)	7.07	6.32	6.63	6.14	6.36	6.14	6.32	6.11
Ratio $\overline{V_2}/\overline{V_1}$	2.65	2.27	2.17	2.07	2.26	2.23	2.23	2.22
Equiv. thickness e (Å)	21.2	15.1	11.3	8.3	12.8	10.1	11.1	9.5

5. Summary and conclusion

5.1. Practical procedure for particle size analysis

In the present article, we have introduced a new quantity directly defined from the projected area and perimeter of a particle: $d_{grain} = 4A/P$. The relevance of this dimension, especially for particles made of grains, emphasizes the central role that perimeter could play (to go beyond the simple use of A to compute a spherical equivalent diameter $D_{sph} = \sqrt{4A/\pi}$) in the equivalent diameter determination of non-spherical particles. As we have demonstrated with a partial coalescence model, the circularity ($C = 4\pi A/P^2$) which is also determined by A and P, can be used to correct the particle sizes estimation in order to better take into account their specific shapes. We have shown that the out-of-plane dimension can be approximated to a high degree of precision by the quantity:

$$d_\alpha = d_{grain}[1 - (1-\alpha)\sqrt{1-C}] \tag{50}$$

then corresponding to an equivalent diameter $D_\alpha = D_{sph}^{2/3} d_\alpha^{1/3}$ much more adapted than the spherical approximation to describe particles of complex geometries, made of several partially coalesced grains. Such a regime is indeed experimentally relevant and can be detected by a linear trend in the A vs P evolution among the particles in an assembly. In this kind of regime, while the grain approximation is adapted for a negligible coalescence parameter, the alpha approximation given above should provide excellent results with a correctly chosen α constant, whose value reflect the coalescence degree. However, the best α value only varies in a limited range (typically between 0.55 and 0.75) so that sticking to $\alpha = 0.65$ (as we did here) is usually satisfying.

On the contrary, if the A vs P evolution exhibits a parabolic trend, then instead of the alpha approximation, the ellipsoidal approximation should be used to infer the particle size from the roundness and the projected area (see Eq. (17)). A simple flowchart is given in Fig. 8, summarizing the procedure to follow in order to reliably determine the particle sizes in a practical case. We hope it will facilitate the use of the present approach, definitely superior to the crude spherical approximation.

5.2. Outlook

The gap between the mean particle size evaluated using the different approximations provides a useful information on which equivalent size can be trusted. Anyway, since the ellipsoidal, grain and alpha

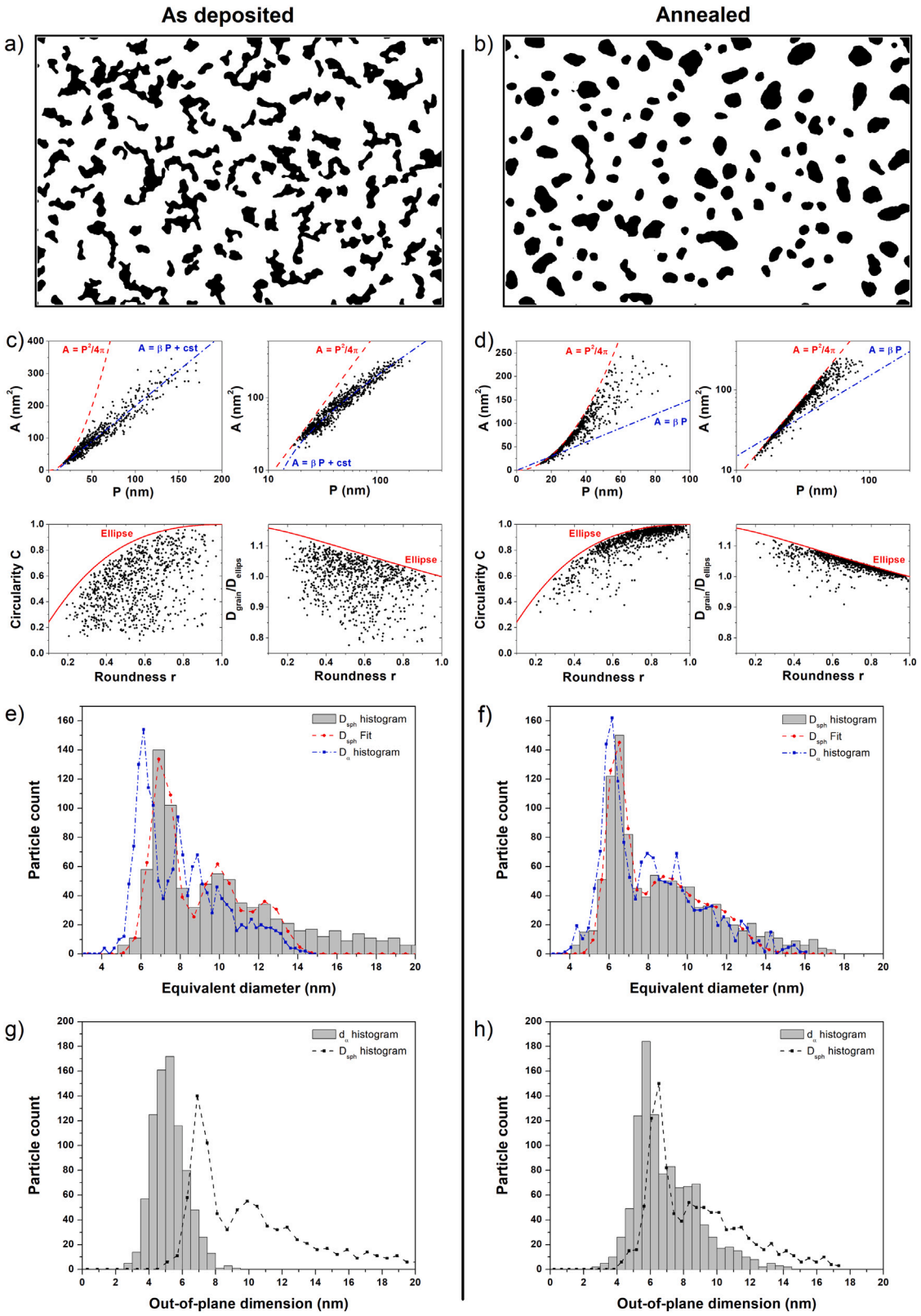

Fig. 7. Analysis of two particles assemblies: as deposited (a, c, e and g) and after annealing (b, d, f and h). (a) and (b) show a typical binary image (size 261 nm × 173 nm); (c) and (d) display the A vs P test (in linear or log scale) as well as C and D_{grain}/D_{ellips} vs roundness r for comparison with the ellipse model (red curves); (e) and (f) display the equivalent diameter histogram (D_{sph} and D_{α}) with an indicative 3-Gaussians fit; (g) and (h) give the out-of-plane dimension histogram (i.e. d_{eq}, approximated by d_{α} with $\alpha = 0.65$), compared to D_{sph} of the spherical approximation.

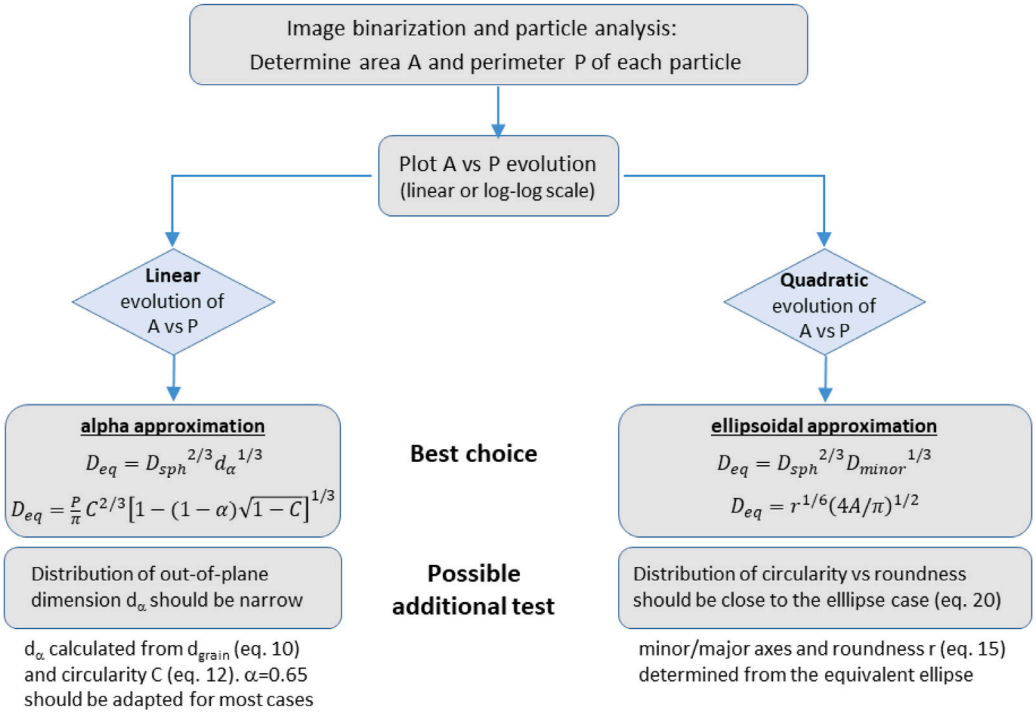

Fig. 8. Flowchart summarizing the approach and the recommendations for a reliable particle size analysis. The keypoint is to separate the two situations: linear or quadratic evolution of A vs P, which indicates if one should use the alpha approximation (Eqs. (43)–(44)) or the ellipsoidal approximation (Eq. (7) or (17)).

approximations encompass the spherical approximation (they all converge to the same value when particles are really spherical), they are always preferable than the crude use of D_{sph}, which unfortunately appears to be standard approach in the nanoparticle community. It must be kept in mind that in most cases the equivalent diameters of the spherical approximation will correspond to an overestimation of the true particle sizes. The resulting error in the particle volume evaluation (and total volume, as expressed by an equivalent thickness) can then be very large, what may subsequently strongly affect and corrupt the determination of other physical quantities. We are convinced that a good knowledge of the particle size in an assembly is a prerequisite for reliable size-effect investigations.

Our simple approach, which propose an efficient way to go beyond the spherical approximation, only implies the perimeter measurement of each particle. This is easily accessible with many image analysis softwares, but we insist on the fact that length evaluation for digitized curves has to be cautiously performed. This is why our advice is to use the *corner-count* estimator [117], for instance proposed in our ParticlesShape plugin for ImageJ. It is remarkable that with a 2D information (giving access to the projected area and perimeter, i.e. also to the circularity parameter), measured with conventional TEM as routine observations on particle assemblies, one has access to an information on the particle thickness (i.e. the out-of-plane dimension). Even if the model could be complexified (non-spherical grains, coalescence description...), the proposed approach has been validated on samples of mass-selected nanoparticles, offering a powerful way to test the adequation of the inferred sizes thanks to the presence of well-defined *n*-mers. The alpha approximation should be adapted for particles made of a few grains (typically of the order of 10 or less) and our model has been devised for grains that are lying in-plane: it was supposed that there is no 3D projection effect (note that two grains of diameter D exactly on top of each other would appear as a single particle of diameter D, this kind of situation is supposed to be excluded or negligible).

Other specific analyses schemes have been proposed for other special cases, such as soot particles with complex 3D shapes (agglomerates of a large number of primary particles, displaying non-integer fractal dimension arrangements), with much more complicated criteria and often supplemented with computer simulations. In the present article, we have shown how to easily improve the reliability of size-histogram determination, on an entire assembly of non-spherical particles, with almost no additional computational expense. Of course there also exist more involved experimental techniques (atom probe or electron tomography, phase contrast imaging, STEM-HAADF etc.) which can provide a 3D information on individual nanoparticles, but they cannot be routinely applied to hundreds of particles! This is why we are convinced that the partial coalescence model, with the alpha approximation that we have introduced, can be useful in a variety of scientific fields (not only for *nano*-particles) when preformed particles are deposited on a surface.

Declaration of competing interest

The authors declare that they have no known competing financial interests or personal relationships that could have appeared to influence the work reported in this paper.

Appendix A. List of variables

See Table A.1.

Appendix B. Supplementary data

Supplementary material related to this article can be found online at https://doi.org/10.1016/j.ultramic.2024.114067.

Data availability

Data will be made available on request.

Table A.1
List of the main variables used in the article, with their physical meaning, the section where they first appear and the equations of figure used for their definition.

Name	Physical meaning	Section	Eq./Fig.
A	projected area of a particle	Section 1	
P	perimeter of a particle	Section 1	
V	volume of a particle	Section 2	
D_{eq}	(volume) equivalent diameter	Section 2.1	Eq. (1)[a]
D_{sph}	spherical equivalent diameter	Section 2.1	Eq. (2)
V_{sph}	hypothetical spherical volume	Section 2.1	Eq. (3)
D_{major}	major axis of the equivalent ellipse	Section 2.2	Fig. 2
D_{minor}	minor axis of the equivalent ellipse	Section 2.2	Fig. 2
V_{ellips}	hypothetical ellipsoidal volume	Section 2.2	Eq. (5)
D_{ellips}	equivalent diameter in the ellipsoidal approx.	Section 2.2	Eqs. (6)–(7)
d_{grain}	grain diameter (without coalescence)	Section 2.3	Fig. 2, Eq. (10)[b]
V_{grain}	hypothetical volume for a particle of n grains	Section 2.3	Eq. (9)
D_{grain}	equivalent diameter in the grain approx.	Section 2.3	Eq. (11)
C	circularity (dimensionless)	Section 2.4	Eq. (12)
r	roundness (dimensionless)	Section 2.4	Eq. (15)
h	overlapping distance for partial coalescence	Section 3	Fig. 3
R_g	radius of partially coalesced spherical grains	Section 3	Fig. 3, Eq. (32)[c]
x	coalescence parameter (dimensionless)	Section 3	
A_n	projected area of a (partially coalesced) n-mer	Section 3.1	
P_n	perimeter of a (partially coalesced) n-mer	Section 3.1	
V_n	volume of a (partially coalesced) n-mer	Section 3.1	Eq. (22)
D	initial diameter of a grain (before coalescence)	Section 3.1	Eq. (22)[d]
A_0	area of a disk of radius R_g	Section 3.1	
P_0	perimeter of a disk of radius R_g	Section 3.1	
V_0	volume of a sphere of radius R_g	Section 3.1	
d_{eq}	out-of-plane dimension relating V_n to A_n	Section 3.2	Eqs. (37)–(38)[e]
d_α	alpha approximation of the true d_{eq}	Section 3.2	Eq. (41)
α	(adjustable) parameter used to express d_α	Section 3.2	Eq. (41)[f]
D_α	equiv. diameter in the alpha approx.	Section 3.2	Eqs. (42)–(44)
H	height of partially coalesced particles	Section 3.4	Eq. (47)

[a] Sometimes called "area-equivalent diameter" since it is only determined from the projected area A.

[b] As expressed by Eq. (10), one can always calculate a value of d_{grain} from A and P.

[c] Its value depends on the number of grains (n) and the coalescence parameter (x).

[d] It is also equal to a monomer diameter, for which we have $D = 2R_g$.

[e] d_{eq} also relates the true D_{eq} to D_{sph}.

[f] α depends on x but in a limited range, so that $\alpha = 0.65$ is a good choice.

References

[1] R. Taylor, S. Coulombe, T. Otanicar, P. Phelan, A. Gunawan, W. Lv, G. Rosengarten, R. Prasher, H. Tyagi, Small particles, big impacts: A review of the diverse applications of nanofluids, J. Appl. Phys. 113 (1) (2013) 011301, http://dx.doi.org/10.1063/1.4754271.

[2] M. De, P.S. Ghosh, V.M. Rotello, Applications of nanoparticles in biology, Adv. Mater. 20 (22) (2008) 4225–4241, http://dx.doi.org/10.1002/adma.200703183.

[3] A. Perez, P. Melinon, V. Dupuis, L. Bardotti, B. Masenelli, F. Tournus, B. Prevel, J.T. Combes, E. Bernstein, A. Tamion, N. Blanc, D. Tainoff, O. Boisron, G. Guiraud, M. Broyer, M. Pellarin, N.D. Fatti, F. Vallee, E. Cottancin, J. Lerme, J.L. Vialle, C. Bonnet, P. Maioli, A. Crut, C. Clavier, J. Rousset, F. Morfin, Functional nanostructures from clusters, Int. J. Nanotechnol. 7 (4/5/6/7/8) (2010) 523, http://dx.doi.org/10.1504/IJNT.2010.031733.

[4] P. Punia, M. Naagar, S. Chalia, R. Dhar, B. Ravelo, P. Thakur, A. Thakur, Recent advances in synthesis, characterization, and applications of nanoparticles for contaminated water treatment- A review, Ceram. Int. 47 (2) (2021) 1526–1550, http://dx.doi.org/10.1016/j.ceramint.2020.09.050.

[5] W. Niu, G. Xu, Crystallographic control of noble metal nanocrystals, Nano Today 6 (3) (2011) 265–285, http://dx.doi.org/10.1016/j.nantod.2011.04.006.

[6] T.A. Sipkens, A. Boies, J.C. Corbin, R.K. Chakrabarty, J. Olfert, S.N. Rogak, Overview of methods to characterize the mass, size, and morphology of soot, J. Aerosol Sci. 173 (2023) 106211, http://dx.doi.org/10.1016/j.jaerosci.2023.106211.

[7] E.A. Coronado, E.R. Encina, F.D. Stefani, Optical properties of metallic nanoparticles: manipulating light, heat and forces at the nanoscale, Nanoscale 3 (10) (2011) 4042, http://dx.doi.org/10.1039/c1nr10788g.

[8] B. Roldan Cuenya, F. Behafarid, Nanocatalysis: size- and shape-dependent chemisorption and catalytic reactivity, Surf. Sci. Rep. 70 (2) (2015) 135–187, http://dx.doi.org/10.1016/j.surfrep.2015.01.001.

[9] M. Sajid, J. Płotka-Wasylka, Nanoparticles: Synthesis, characteristics, and applications in analytical and other sciences, Microchem. J. 154 (2020) 104623, http://dx.doi.org/10.1016/j.microc.2020.104623.

[10] S. Singamaneni, V.N. Bliznyuk, C. Binek, E.Y. Tsymbal, Magnetic nanoparticles: recent advances in synthesis, self-assembly and applications, J. Mater. Chem. 21 (42) (2011) 16819, http://dx.doi.org/10.1039/c1jm11845e.

[11] D.J. Sellmyer, B. Balamurugan, B. Das, P. Mukherjee, R. Skomski, G.C. Hadjipanayis, Novel structures and physics of nanomagnets (invited), J. Appl. Phys. 117 (17) (2015) 172609, http://dx.doi.org/10.1063/1.4914339.

[12] S. Bourrous, Q. Ribeyre, L. Lintis, J. Yon, S. Bau, D. Thomas, C. Vallières, F.-X. Ouf, A semi-automatic analysis tool for the determination of primary particle size, overlap coefficient and specific surface area of nanoparticles aggregates, J. Aerosol Sci. 126 (2018) 122–132, http://dx.doi.org/10.1016/j.jaerosci.2018.09.001.

[13] H. Bresch, V.-D. Hodoroaba, A. Schmidt, K. Rasmussen, H. Rauscher, Counting small particles in electron microscopy images—Proposal for rules and their application in practice, Nanomaterials 12 (13) (2022) 2238, http://dx.doi.org/10.3390/nano12132238.

[14] E.A. Grulke, K. Yamamoto, K. Kumagai, I. Häusler, W. Österle, E. Ortel, V.-D. Hodoroaba, S.C. Brown, C. Chan, J. Zheng, K. Yamamoto, K. Yashiki, N.W. Song, Y.H. Kim, A.B. Stefaniak, D. Schwegler-Berry, V.A. Coleman, A.s.K. Jämting, J. Herrmann, T. Arakawa, W.W. Burchett, J.W. Lambert, A.J. Stromberg, Size and shape distributions of primary crystallites in titania aggregates, Adv. Powder Technol. 28 (7) (2017) 1647–1659, http://dx.doi.org/10.1016/j.apt.2017.03.027.

[15] T. Klein, E. Buhr, K.-P. Johnsen, C.G. Frase, Traceable measurement of nanoparticle size using a scanning electron microscope in transmission mode (TSEM), Meas. Sci. Technol. 22 (9) (2011) 094002, http://dx.doi.org/10.1088/0957-0233/22/9/094002.

[16] F. Meli, T. Klein, E. Buhr, C.G. Frase, G. Gleber, M. Krumrey, A. Duta, S. Duta, V. Korpelainen, R. Bellotti, G.B. Picotto, R.D. Boyd, A. Cuenat, Traceable size determination of nanoparticles, a comparison among European metrology institutes, Meas. Sci. Technol. 23 (12) (2012) 125005, http://dx.doi.org/10.1088/0957-0233/23/12/125005.

[17] L. Gentile, H. Mateos, A. Mallardi, M. Dell'Aglio, A. De Giacomo, N. Cioffi, G. Palazzo, Gold nanoparticles obtained by ns-pulsed laser ablation in liquids (ns-PLAL) are arranged in the form of fractal clusters, J. Nanoparticle Res. 23 (2) (2021) 35, http://dx.doi.org/10.1007/s11051-021-05140-5.

[18] A. Hillion, A. Tamion, F. Tournus, C. Albin, V. Dupuis, From vanishing interaction to superferromagnetic dimerization: Experimental determination of interaction lengths for embedded Co clusters, Phys. Rev. B 95 (13) (2017) 134446, http://dx.doi.org/10.1103/PhysRevB.95.134446.

[19] F. Tournus, N. Blanc, A. Tamion, M. Hillenkamp, V. Dupuis, Synthesis and magnetic properties of size-selected CoPt nanoparticles, J. Magn. Magn. Mater. 323 (14) (2011) 1868–1872, http://dx.doi.org/10.1016/j.jmmm.2011.02.024.

[20] F. Tournus, A. Tamion, N. Blanc, A. Hillion, V. Dupuis, Signature of multimers on magnetic susceptibility curves for mass-selected Co particles, J. Appl. Phys. 109 (7) (2011) 07B502, http://dx.doi.org/10.1063/1.3535554.

[21] S. Oyarzún, A. Tamion, F. Tournus, V. Dupuis, M. Hillenkamp, Size effects in the magnetic anisotropy of embedded cobalt nanoparticles: from shape to surface, Sci. Rep. 5 (1) (2015) 14749, http://dx.doi.org/10.1038/srep14749.

[22] V. Dupuis, A. Hillion, A. Robert, O. Loiselet, G. Khadra, P. Capiod, C. Albin, O. Boisron, D. Le Roy, L. Bardotti, F. Tournus, A. Tamion, Bottom-up strategies for the assembling of magnetic systems using nanoclusters, J. Nanoparticle Res. 20 (5) (2018) 128, http://dx.doi.org/10.1007/s11051-018-4189-3.

[23] V. Dupuis, G. Khadra, J.M. Montejano-Carrizales, F. Tournus, F. Aguilera-Granja, A. Tamion, Mass-selected FeCo clusters embedded in a carbon matrix as benchmark nanocatalysts, ACS Appl. Nano Mater. 2 (5) (2019) 2864–2872, http://dx.doi.org/10.1021/acsanm.9b00313.

[24] B.M. Lacava, R.B. Azevedo, L.P. Silva, Z.G.M. Lacava, K.S. Neto, N. Buske, A.F. Bakuzis, P.C. Morais, Particle sizing of magnetite-based magnetic fluid using atomic force microscopy: A comparative study with electron microscopy and birefringence, Appl. Phys. Lett. 77 (12) (2000) 1876–1878, http://dx.doi.org/10.1063/1.1311320.

[25] J.T. Batley, M. Nguyen, I. Kamboj, C. Korostynski, E.S. Aydil, C. Leighton, Quantitative understanding of superparamagnetic blocking in thoroughly characterized Ni nanoparticle assemblies, Chem. Mater. 32 (15) (2020) 6494–6506, http://dx.doi.org/10.1021/acs.chemmater.0c01758.

[26] A. Bertran, S. Sandoval, J. Oró-Solé, À. Sánchez, G. Tobias, Particle size determination from magnetization curves in reduced graphene oxide decorated with monodispersed superparamagnetic iron oxide nanoparticles, J. Colloid Interface Sci. 566 (2020) 107–119, http://dx.doi.org/10.1016/j.jcis.2020.01.072.

[27] U. Klekotka, B. Piotrowska, D. Satuł a, B. Kalska-Szostko, Modified ferrite core-shell nanoparticles magneto-structural characterization, Appl. Surf. Sci. 444 (2018) 161–167, http://dx.doi.org/10.1016/j.apsusc.2018.02.212.

[28] S.B. Rice, C. Chan, S.C. Brown, P. Eschbach, L. Han, D.S. Ensor, A.B. Stefaniak, J. Bonevich, A.E. Vladár, A.R.H. Walker, J. Zheng, C. Starnes, A. Stromberg, J. Ye, E.A. Grulke, Particle size distributions by transmission electron microscopy: an interlaboratory comparison case study, Metrologia 50 (6) (2013) 663–678, http://dx.doi.org/10.1088/0026-1394/50/6/663.

[29] J. Feng, G. Biskos, A. Schmidt-Ott, Toward industrial scale synthesis of ultrapure singlet nanoparticles with controllable sizes in a continuous gas-phase process, Sci. Rep. 5 (1) (2015) 15788, http://dx.doi.org/10.1038/srep15788.

[30] P. Eaton, P. Quaresma, C. Soares, C. Neves, M.P. de Almeida, E. Pereira, P. West, A direct comparison of experimental methods to measure dimensions of synthetic nanoparticles, Ultramicroscopy 182 (2017) 179–190, http://dx.doi.org/10.1016/j.ultramic.2017.07.001.

[31] K. Heinemann, F. Soria, On the detection and size classification of nanometer-size metal particles on amorphous substrates, Ultramicroscopy 20 (1) (1986) 1–14, http://dx.doi.org/10.1016/0304-3991(86)90161-0.

[32] M. Mirzaei, H.K. Rafsanjani, An automatic algorithm for determination of the nanoparticles from TEM images using circular hough transform, Micron 96 (2017) 86–95, http://dx.doi.org/10.1016/j.micron.2017.02.008.

[33] L. Crouzier, A. Delvallée, S. Ducourtieux, L. Devoille, C. Tromas, N. Feltin, A new method for measuring nanoparticle diameter from a set of SEM images using a remarkable point, Ultramicroscopy 207 (2019) 112847, http://dx.doi.org/10.1016/j.ultramic.2019.112847.

[34] G. Dahy, M.M. Soliman, H. Alshater, A. Slowik, A. Ella Hassanien, Optimized deep networks for the classification of nanoparticles in scanning electron microscopy imaging, Comput. Mater. Sci. 223 (2023) 112135, http://dx.doi.org/10.1016/j.commatsci.2023.112135.

[35] M.R. Cox, M. Budhu, A practical approach to grain shape quantification, Eng. Geol. 96 (1–2) (2008) 1–16, http://dx.doi.org/10.1016/j.enggeo.2007.05.005.

[36] E.C. Crawford, J.K. Mortensen, An ImageJ plugin for the rapid morphological characterization of separated particles and an initial application to placer gold analysis, Comput. Geosci. 35 (2) (2009) 347–359, http://dx.doi.org/10.1016/j.cageo.2007.11.012.

[37] M. Đuriš, Z. Arsenijević, D. Jaćimovski, T. Kaluđerović Radoičić, Optimal pixel resolution for sand particles size and shape analysis, Powder Technol. 302 (2016) 177–186, http://dx.doi.org/10.1016/j.powtec.2016.08.045.

[38] D.L. Galata, L.A. Mészáros, N. Kállai-Szabó, E. Szabó, H. Pataki, G. Marosi, Z.K. Nagy, Applications of machine vision in pharmaceutical technology: A review, Eur. J. Pharm. Sci. 159 (2021) 105717, http://dx.doi.org/10.1016/j.ejps.2021.105717.

[39] C. Igathinathane, L. Pordesimo, E. Columbus, W. Batchelor, S. Methuku, Shape identification and particles size distribution from basic shape parameters using ImageJ, Comput. Electron. Agric. 63 (2) (2008) 168–182, http://dx.doi.org/10.1016/j.compag.2008.02.007.

[40] C. Igathinathane, S. Melin, S. Sokhansanj, X. Bi, C. Lim, L. Pordesimo, E. Columbus, Machine vision based particle size and size distribution determination of airborne dust particles of wood and bark pellets, Powder Technol. 196 (2) (2009) 202–212, http://dx.doi.org/10.1016/j.powtec.2009.07.024.

[41] Y. Kim, G. Dodbiba, A novel method for simultaneous evaluation of particle geometry by using image processing analysis, Powder Technol. 393 (2021) 60–73, http://dx.doi.org/10.1016/j.powtec.2021.07.058.

[42] D. Legland, J. Beaugrand, Automated clustering of lignocellulosic fibres based on morphometric features and using clustering of variables, Ind. Crop. Prod. 45 (2013) 253–261, http://dx.doi.org/10.1016/j.indcrop.2012.12.021.

[43] D. Legland, I. Arganda-Carreras, P. Andrey, MorphoLibJ: integrated library and plugins for mathematical morphology with ImageJ, Bioinformatics 32 (22) (2016) 3532–3534, http://dx.doi.org/10.1093/bioinformatics/btw413.

[44] S. Leibrandt, J.-L. Le Pennec, Towards fast and routine analyses of volcanic ash morphometry for eruption surveillance applications, J. Volcanol. Geotherm. Res. 297 (2015) 11–27, http://dx.doi.org/10.1016/j.jvolgeores.2015.03.014.

[45] A.I. Medalia, Morphology of agreggates. I. calculation of shape and Bulkiness-Factors; Application to computer-simulated random flocs, J. Colloid Interface Sci. 24 (1967) 393.

[46] A.I. Medalia, Morphology of agreggates. VI. Effective volume of aggregates of carbon black from electron microscopy; Application to vehicle absorption and to die swell of filled rubber I, 2, J. Colloid Interface Sci. 32 (1) (1970) 115.

[47] E. Verleysen, T. Wagner, H.-G. Lipinski, R. Kägi, R. Koeber, A. Boix-Sanfeliu, P.-J. De Temmerman, J. Mast, Evaluation of a TEM based approach for size measurement of particulate (nano)materials, Materials 12 (14) (2019) 2274, http://dx.doi.org/10.3390/ma12142274.

[48] J.C. Dur, The relationship between particle-size distribution by laser granulometry and image analysis by transmission electron microscopy in a soil clay fraction, Eur. J. Soil Sci. 55 (2004) 265, http://dx.doi.org/10.1111/j.1365-2389.2004.00597.x.

[49] P. Donnadieu, S. Lazar, G.A. Botton, I. Pignot-Paintrand, M. Reynolds, S. Perez, Seeing structures and measuring properties with transmission electron microscopy images: A simple combination to study size effects in nanoparticle systems, Appl. Phys. Lett. 94 (26) (2009) 263116, http://dx.doi.org/10.1063/1.3168525.

[50] A. Verguet, C. Messaoudi, S. Marco, P. Donnadieu, An ImageJ tool for simplified post-treatment of TEM phase contrast images (SPCI), Micron 121 (2019) 90–98, http://dx.doi.org/10.1016/j.micron.2019.01.006.

[51] P. Banerjee, C. Roy, S.K. De, A.J. Santos, F.M. Morales, S. Bhattacharyya, Atomically resolved tomographic reconstruction of nanoparticles from single projection: Influence of amorphous carbon support, Ultramicroscopy 221 (2021) 113177, http://dx.doi.org/10.1016/j.ultramic.2020.113177.

[52] F.-R. Chen, D. Van Dyck, C. Kisielowski, In-line three-dimensional holography of nanocrystalline objects at atomic resolution, Nature Commun. 7 (1) (2016) 10603, http://dx.doi.org/10.1038/ncomms10603.

[53] A. De Backer, S. Bals, S. Van Aert, A decade of atom-counting in STEM: From the first results toward reliable 3D atomic models from a single projection, Ultramicroscopy 247 (2023) 113702, http://dx.doi.org/10.1016/j.ultramic.2023.113702.

[54] S.D. House, Y. Chen, R. Jin, J.C. Yang, High-throughput, semi-automated quantitative STEM mass measurement of supported metal nanoparticles using a conventional TEM/STEM, Ultramicroscopy 182 (2017) 145–155, http://dx.doi.org/10.1016/j.ultramic.2017.07.004.

[55] S.D. House, C.S. Bonifacio, R.V. Grieshaber, L. Li, Z. Zhang, J. Ciston, E.A. Stach, J.C. Yang, Statistical analysis of support thickness and particle size effects in HRTEM imaging of metal nanoparticles, Ultramicroscopy 169 (2016) 22–29, http://dx.doi.org/10.1016/j.ultramic.2016.06.007.

[56] V. Gasnier, B. Gault, H. Nako, Y. Aruga, G. Sha, S.P. Ringer, Influence of experimental parameters on the composition of precipitates in metallic alloys, IFES 2012, Ultramicroscopy 132 (2013) 199–204, http://dx.doi.org/10.1016/j.ultramic.2013.02.005.

[57] B. Goris, T. Roelandts, K.J. Batenburg, H. Heidari Mezerji, S. Bals, Advanced reconstruction algorithms for electron tomography: From comparison to combination, Frontiers of Electron Microscopy in Materials Science, Ultramicroscopy 127 (2013) 40–47, http://dx.doi.org/10.1016/j.ultramic.2012.07.003.

[58] M. Hayashida, F. Paraguay-Delgado, C. Ornelas, A. Herzing, A.M. Blackburn, B. Haydon, T. Yaguchi, A. Wakui, K. Igarashi, Y. Suzuki, S. Motoki, Y. Aoyama, Y. Konyuba, M. Malac, Nanoparticle size and 3D shape measurement by electron tomography: An inter-laboratory comparison, Micron 140 (2021) 102956, http://dx.doi.org/10.1016/j.micron.2020.102956.

[59] S.V.N.T. Kuchibhatla, V. Shutthanandan, T.J. Prosa, P. Adusumilli, B. Arey, A. Buxbaum, Y.C. Wang, T. Tessner, R. Ulfig, C.M. Wang, S. Thevuthasan, Three-dimensional chemical imaging of embedded nanoparticles using atom probe tomography, Nanotechnology 23 (21) (2012) 215704, http://dx.doi.org/10.1088/0957-4484/23/21/215704.

[60] C.A. Little, C. Batchelor-McAuley, N.P. Young, R.G. Compton, Shape and size of non-spherical silver nanoparticles: implications for calculating nanoparticle number concentrations, Nanoscale 10 (34) (2018) 15943–15947, http://dx.doi.org/10.1039/C8NR06062B.

[61] R.K.W. Marceau, L.T. Stephenson, C.R. Hutchinson, S.P. Ringer, Quantitative atom probe analysis of nanostructure containing clusters and precipitates with multiple length scales, Special Issue: 52nd International Field Emission Symposium, Ultramicroscopy 111 (6) (2011) 738–742, http://dx.doi.org/10.1016/j.ultramic.2010.12.029.

[62] S. Sueda, K. Yoshida, N. Tanaka, Quantification of metallic nanoparticle morphology on TiO2 using HAADF-STEM tomography, Ultramicroscopy 110 (9) (2010) 1120–1127, http://dx.doi.org/10.1016/j.ultramic.2010.04.003.

[63] S.-H. Kim, P.W. Kang, O.O. Park, J.-B. Seol, J.-P. Ahn, J.Y. Lee, P.-P. Choi, A new method for mapping the three-dimensional atomic distribution within nanoparticles by atom probe tomography (APT), Ultramicroscopy 190 (2018) 30–38, http://dx.doi.org/10.1016/j.ultramic.2018.04.005.

[64] C. Zelenka, M. Kamp, K. Strohm, A. Kadoura, J. Johny, R. Koch, L. Kienle, Automated classification of nanoparticles with various ultrastructures and sizes via deep learning, Ultramicroscopy 246 (2023) 113685, http://dx.doi.org/10.1016/j.ultramic.2023.113685.

[65] A. Bescond, J. Yon, F.X. Ouf, D. Ferry, D. Delhaye, D. Gaffié, A. Coppalle, C. Rozé, Automated determination of aggregate primary particle size distribution by TEM image analysis: Application to soot, Aerosol Sci. Technol. 48 (8) (2014) 831–841, http://dx.doi.org/10.1080/02786826.2014.932896.

[66] D. Lottin, D. Ferry, J.-M. Gay, D. Delhaye, F.-X. Ouf, On methods determining the fractal dimension of combustion aerosols and particleclusters, J. Aerosol Sci. 58 (2013) 41–49, http://dx.doi.org/10.1016/j.jaerosci.2012.12.009.

[67] P.-J. De Temmerman, E. Verleysen, J. Lammertyn, J. Mast, Semi-automatic size measurement of primary particles in aggregated nanomaterials by transmission electron microscopy, Powder Technol. 261 (2014) 191–200, http://dx.doi.org/10.1016/j.powtec.2014.04.040.

[68] R. Dastanpour, J.M. Boone, S.N. Rogak, Automated primary particle sizing of nanoparticle aggregates by TEM image analysis, Powder Technol. 295 (2016) 218–224, http://dx.doi.org/10.1016/j.powtec.2016.03.027.

[69] M. Frei, F.E. Kruis, Fully automated primary particle size analysis of agglomerates on transmission electron microscopy images via artificial neural networks, Powder Technol. 332 (2018) 120–130, http://dx.doi.org/10.1016/j.powtec.2018.03.032.

[70] F. Tournus, Multimer formation for two-dimensional random nanoparticle deposition, Phys. Rev. E 84 (1) (2011) 011612, http://dx.doi.org/10.1103/PhysRevE.84.011612.

[71] As noted by Litster and Ennis [121], “The equivalent diameter is the diameter of a sphere with the same property as the particle eg. the volume equivalent diameter is the diameter of a sphere with the same volume as the particle”.

[72] C. Becke, M. Schumann, J. Geist, A. Brinker, Shape characteristics of suspended solids and implications in different salmonid aquaculture production systems, Aquaculture 516 (2020) 734631, http://dx.doi.org/10.1016/j.aquaculture.2019.734631.

[73] N. Feltin, A. Delvallée, L.c. Crouzier, Strategy for ensuring the metrological traceability of nanoparticle size measurements by SEM, Nanomaterials 14 (11) (2024) 931, http://dx.doi.org/10.3390/nano14110931.

[74] E.A. Grulke, S.B. Rice, J. Xiong, K. Yamamoto, T.H. Yoon, K. Thomson, M. Saffaripour, G.J. Smallwood, J.W. Lambert, A.J. Stromberg, R. Macy, N.J. Briot, D. Qian, Size and shape distributions of carbon black aggregates by transmission electron microscopy, Carbon 130 (2018) 822–833, http://dx.doi.org/10.1016/j.carbon.2018.01.030.

[75] C. Hegel, C. Jones, F. Cabrera, M.J. Yáñez, V. Bucala, Particle size characterization: comparison of laser difraction (LD) and scanning electron microscopy (SEM), Acta Microsc. 23 (1) (2014) 11.

[76] A.Y. Kharin, Deep learning for scanning electron microscopy: Synthetic data for the nanoparticles detection, Ultramicroscopy 219 (2020) 113125, http://dx.doi.org/10.1016/j.ultramic.2020.113125.

[77] L. Cervera Gontard, D. Ozkaya, R.E. Dunin-Borkowski, A simple algorithm for measuring particle size distributions on an uneven background from TEM images, Ultramicroscopy 111 (2) (2011) 101–106, http://dx.doi.org/10.1016/j.ultramic.2010.10.011.

[78] S.L. Cheng, S.L. Wong, S.W. Lu, H. Chen, Large-area Co-silicide nanodot arrays produced by colloidal nanosphere lithography and thermal annealing, Ultramicroscopy 108 (10) (2008) 1200–1204, http://dx.doi.org/10.1016/j.ultramic.2008.04.065.

[79] As noted by Rice others, [28], "ISO standards have been developed for the area-equivalent diameter measurements of powders but do not specifically refer to nanoparticles.".

[80] L.D. Marks, L. Peng, Nanoparticle shape, thermodynamics and kinetics, J. Phys.: Condens. Matter. 28 (5) (2016) 053001, http://dx.doi.org/10.1088/0953-8984/28/5/053001.

[81] F. Baletto, R. Ferrando, Structural properties of nanoclusters: Energetic, thermodynamic, and kinetic effects, Rev. Modern Phys. 77 (1) (2005) 371–423, http://dx.doi.org/10.1103/RevModPhys.77.371.

[82] J. Kim, D. Kang, S. Kang, B.H. Kim, J. Park, Coalescence dynamics of platinum group metal nanoparticles revealed by liquid-phase transmission electron microscopy, iScience 25 (8) (2022) 104699, http://dx.doi.org/10.1016/j.isci.2022.104699.

[83] A. Reyes, G. Herrera, P. Capiod, D. Le Roy, V. Dupuis, I. Cañero-Infante, G. Saint-Girons, R. Bachelet, A. Resta, P. Ohresser, L. Martinelli, X. Weng, G. Renaud, F. Tournus, Preferential orientations of FeRh nanomagnets deposited on a BaTiO 3 epitaxial thin film, Phys. Rev. B 109 (24) (2024) 245410, http://dx.doi.org/10.1103/PhysRevB.109.245410.

[84] M.J. Rhodes, K.P. Hapgood (Eds.), Introduction to Particle Technology, 2. ed, Wiley, Weinheim, 2008.

[85] L. Banta, K. Cheng, J. Zaniewski, Estimation of limestone particle mass from 2D images, Powder Technol. 132 (2–3) (2003) 184–189, http://dx.doi.org/10.1016/S0032-5910(03)00061-5.

[86] L. Bardotti, F. Tournus, C. Albin, O. Boisron, V. Dupuis, Self-organisation of size-selected co_xpt_{1-x} clusters on graphite, Phys. Chem. Chem. Phys. 16 (48) (2014) 26653–26657, http://dx.doi.org/10.1039/C4CP02119C.

[87] L. Bardotti, F. Tournus, M. Pellarin, M. Broyer, P. Mélinon, V. Dupuis, Spontaneous formation of size-selected bimetallic nanoparticle arrays, Surf. Sci. 606 (1–2) (2012) 110–114, http://dx.doi.org/10.1016/j.susc.2011.09.010.

[88] K.C. Lai, Y. Han, P. Spurgeon, W. Huang, P.A. Thiel, D.-J. Liu, J.W. Evans, Reshaping, intermixing, and coarsening for metallic nanocrystals: Nonequilibrium statistical mechanical and coarse-grained modeling, Chem. Rev. 119 (11) (2019) 6670–6768, http://dx.doi.org/10.1021/acs.chemrev.8b00582.

[89] R. Alayan, L. Arnaud, M. Broyer, E. Cottancin, J. Lermé, J.L. Vialle, M. Pellarin, Morphology and growth of metal clusters in the gas phase: A transition from spherical to ramified structures, Phys. Rev. B 73 (12) (2006) 125444, http://dx.doi.org/10.1103/PhysRevB.73.125444.

[90] S. Tsyganov, J. Kästner, B. Rellinghaus, T. Kauffeldt, F. Westerhoff, D. Wolf, Analysis of Ni nanoparticle gas phase sintering, Phys. Rev. B 75 (4) (2007) 045421, http://dx.doi.org/10.1103/PhysRevB.75.045421.

[91] One has to pay attention to the definition of the *circularity* since some authors [44,74] use a definition which is equivalent to the square root of the one we use in the present article, or even another one [72].

[92] T. Muir, Formula for the perimeter of an ellipse, Nature 66 (1703) (1902) 174.

[93] Let us mention two other approximate expressions, the classical one (attributed to Euler) where $P \simeq \pi\sqrt{(D_{major}^2 + D_{minor}^2)/2}$ gives $C_{ellips} \simeq 2r/(1+r^2)$ and the much more precise one, due to Ramanujan where $P \simeq (\pi D_{major}/2)[3(1+r) - \sqrt{(3+r)(1+3r)}]$ corresponds to $C_{ellips} \simeq 4r/[3(1+r) - \sqrt{(3+r)(1+3r)}]^2$. The expression from Muir in the text is alsmost as precise as the one of Ramanujan. See for instance https://www.numericana.com/answer/ellipse.htm.

[94] Another equivalent way to test the existence of a well-defined d_{grain} value is to plot the circularity C as a function of the inverse perimeter: we can write $C = \pi d_{grain}/P$ so that C varies linearly with $1/P$ if d_{grain} is a constant..

[95] D.N. McCarthy, S.A. Brown, Evolution of neck radius and relaxation of coalescing nanoparticles, Phys. Rev. B 80 (6) (2009) 064107, http://dx.doi.org/10.1103/PhysRevB.80.064107.

[96] M.L. Eggersdorfer, D. Kadau, H.J. Herrmann, S.E. Pratsinis, Multiparticle sintering dynamics: From fractal-like aggregates to compact structures, Langmuir 27 (10) (2011) 6358–6367, http://dx.doi.org/10.1021/la200546g.

[97] L. Jiang, Y. Guo, Z. Liu, S. Chen, Computational understanding of the coalescence of metallic nanoparticles: a mini review, Nanoscale 16 (11) (2024) 5521–5536, http://dx.doi.org/10.1039/D3NR06133G.

[98] P. Grammatikopoulos, M. Sowwan, J. Kioseoglou, Computational modeling of nanoparticle coalescence, Adv. Theory and Simul. 2 (6) (2019) 1900013, http://dx.doi.org/10.1002/adts.201900013.

[99] L. Bajtošová, B. Kihoulou, R. Králík, J. Hanuš, M. Cieslar, Nickel nanoparticles: Insights into sintering dynamics, Crystals 14 (4) (2024) 321, http://dx.doi.org/10.3390/cryst14040321.

[100] For special cases, using for instance particles on anisotropic substrates, the equilibrium shapes could significantly deviate from disks. This is also the case when surface energies results in shapes, like cubes, which can hardly be approximated by spheres....

[101] A.M. Brasil, T.L. Farias, M.G. Carvalho, A recipe for image characterization of fractal-like aggregates, J. Aerosol Sci. 30 (10) (1999) 1379, http://dx.doi.org/10.1016/S0021-8502(99)00026-9.

[102] M. Wozniak, F. Onofri, S. Barbosa, J. Yon, J. Mroczka, Comparison of methods to derive morphological parameters of multi-fractal samples of particle aggregates from TEM images, J. Aerosol Sci. 47 (2012) 12–26, http://dx.doi.org/10.1016/j.jaerosci.2011.12.008.

[103] A. Bescond, J. Yon, T. Girasole, C. Jouen, C. Rozé, A. Coppalle, Numerical investigation of the possibility to determine the primary particle size of fractal aggregates by measuring light depolarization, J. Quant. Spectrosc. Radiat. Transfer 126 (2013) 130–139, http://dx.doi.org/10.1016/j.jqsrt.2012.10.011.

[104] In the analysis of TEM images of soot particles, since the projected area only is visible, there is also an apparent overlap due to the 3D structure of the agglomerates. Though it is related to the "real" overlap parameter (which reflects a partial coalescence), the two parameters need to be distinguished [101,102].

[105] Let us insist that the labels "monomer", "dimer" etc. are here related to the number of grains constituting the particle, and not to the fact that they correspond respectively to one incident particle on the surface (deposited cluster size in the case of cluster deposition on a substrate) or two incident/preformed particles which have come into contact (just randomly or after a diffusion/agglomeration process) [70].

[106] See https://doi.org/10.1016/j.ultramic.2024.114067 for supplementary information (best α value and A_2/A_1 ratio evolution; particle height; example of nearly-spherical Pb particles; and ParticlesShape java plugin.

[107] We here suppose that single particles are made of $n_{min} = 1$ grain. More precisely the mean values $\overline{A_2}$ and $\overline{A_1}$ can be used to compute the ratio.

[108] S. Linas, F. Jean, T. Zhou, C. Albin, G. Renaud, L. Bardotti, F. Tournus, Moiré induced organization of size-selected Pt clusters soft landed on epitaxial graphene, Sci. Rep. 5 (1) (2015) 13053, http://dx.doi.org/10.1038/srep13053.

[109] L.L. Wang, X.C. Ma, Y. Qi, P. Jiang, J.F. Jia, Q.K. Xue, J. Jiao, X.H. Bao, Controlled growth of uniform silver clusters on HOPG, Proceedings of the Sixth International Conference on Scanning Probe Microscopy, Sensors and Nanostructures, Ultramicroscopy 105 (1) (2005) 1–5, http://dx.doi.org/10.1016/j.ultramic.2005.06.009.

[110] J. Guckel, M. Görke, G. Garnweitner, D. Park, Smart iterative analysis tool for the size distribution of spherical nanoparticles, Microsc. Microanal. 29 (3) (2023) 1062–1070, http://dx.doi.org/10.1093/micmic/ozad036.

[111] F. Soria, P. Artal, J. Bescos, K. Heinemann, Digital image processing of nanometer-size metal particles on amorphous substrates, Ultramicroscopy 24 (1) (1988) 19–25, http://dx.doi.org/10.1016/0304-3991(88)90323-3.

[112] P. Soille, Morphological image analysis, Springer Berlin Heidelberg, Berlin, Heidelberg, 2004, http://dx.doi.org/10.1007/978-3-662-05088-0.

[113] H. Freeman, Boundary encoding and processing, in: B. Lipkin, A. Rosenfeld (Eds.), Picture Processing and Psychopictorics, Academic Press, New York, NY, 1970, pp. 241–266.

[114] Z. Kulpa, Area and perimeter measurement of blobs in discrete binary pictures, Comput. Graph. Image Process. 6 (5) (1977) 434–451, http://dx.doi.org/10.1016/S0146-664X(77)80021-X.

[115] I. Nyström (Ed.), Discrete geometry for computer imagery: 11th international conference, Naples, Italy, November 19-21, 2003 ; proceedings, Lecture Notes in Computer Science, (2886) DGCI, Springer, 2003, Meeting Name.

[116] G. Bertrand, A. Imiya, R. Klette (Eds.), Digital and image geometry: advanced lectures, Lecture Notes in Computer Science, (2243) ocm48928617, Springer, 2001, OCLC.

[117] L. Dorst, A.W. Smeulders, Length estimators for digitized contours, Comput. Vis. Graph. Image Process. 40 (3) (1987) 311–333, http://dx.doi.org/10.1016/S0734-189X(87)80145-7.

[118] D. Coeurjolly, R. Klette, A comparative evaluation of length estimators of digital curves, IEEE Trans. Pattern Anal. Mach. Intell. 26 (2) (2004) 252–258, http://dx.doi.org/10.1109/TPAMI.2004.1262194.

[119] By G. Landini, see https://blog.bham.ac.uk/intellimic/g-landini-software/.

[120] M. Tajine, A. Daurat, On local definitions of length of digital curves, in: G. Goos, J. Hartmanis, J. Van Leeuwen, I. Nyström, G. Sanniti Di Baja, S. Svensson (Eds.), Discrete Geometry for Computer Imagery, vol. 2886, Lecture Notes in Computer Science, Springer Berlin Heidelberg, 2003, pp. 114–123, http://dx.doi.org/10.1007/978-3-540-39966-7-10, Series Title.

[121] J. Litster, B. Ennis, The science and engineering of granulation processes, Particle Technology Series, vol. 15, Springer Netherlands, Dordrecht, 2004, http://dx.doi.org/10.1007/978-94-017-0546-2.